Article

Cell Reports

Exercise Alleviates Obesity-Induced Metabolic Dysfunction via Enhancing FGF21 Sensitivity in Adipose Tissues

Graphical Abstract

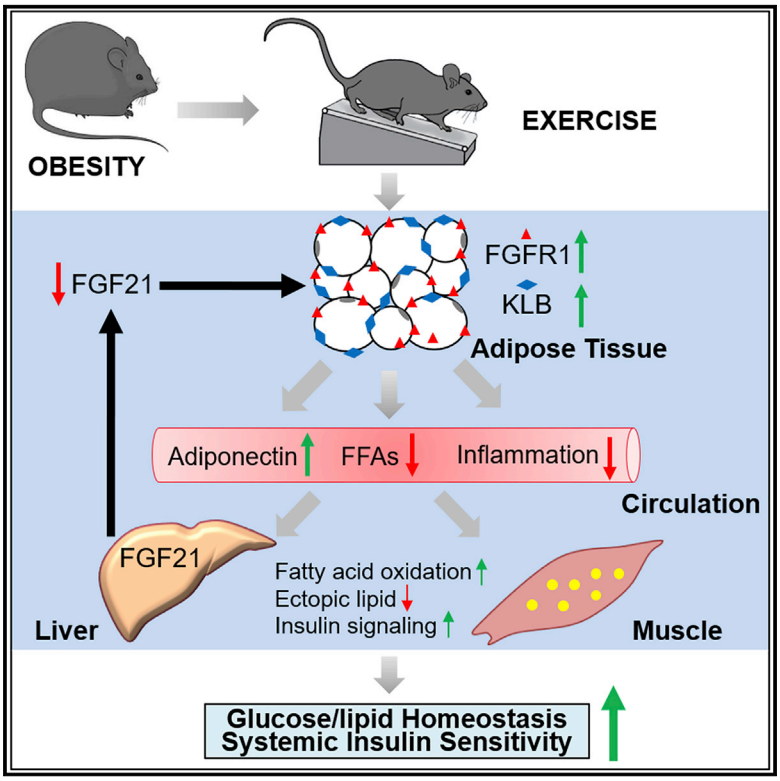

Highlights

- Long-term high fat diet impairs FGF21 sensitivity in adipose tissues
- Exercise reverses diet-induced adipose FGF21 resistance by inducing FGFR1 and KLB
- Mice lacking adipose KLB are refractory to the metabolic benefits of exercise
- Exercise-induced adipose FGFR1 and KLB depends on PPARγ

Authors

Leiluo Geng, Boya Liao, Leigang Jin, ..., Yu Huang, Zhuofeng Lin, Aimin Xu

Correspondence

zhuofenglin@wzmc.edu.cn (Z.L.), amxu@hku.hk (A.X.)

In Brief

Geng et al. identify FGF21 signaling in adipose tissues as an obligatory molecular transducer of exercise, conferring its metabolic benefits on systemic glucose and lipid metabolism and insulin sensitivity. Exercise sensitizes FGF21 actions in adipose tissues, which in turns sends humoral signals to coordinate multi-organ crosstalk for maintaining metabolic homeostasis.

Geng et al., 2019, Cell Reports *26*, 2738–2752
March 5, 2019
https://doi.org/10.1016/j.celrep.2019.02.014

CellPress

OPEN ACCESS
CellPress

Cell Reports
Article

Exercise Alleviates Obesity-Induced Metabolic Dysfunction via Enhancing FGF21 Sensitivity in Adipose Tissues

Leiluo Geng,[1,2] Boya Liao,[1,3] Leigang Jin,[1,3] Zhe Huang,[1,2] Chris R. Triggle,[4] Hong Ding,[4] Jialiang Zhang,[1,2] Yu Huang,[5] Zhuofeng Lin,[1,6,*] and Aimin Xu[1,2,3,7,*]

[1]State Key Laboratory of Pharmaceutical Biotechnology, The University of Hong Kong, Hong Kong, China
[2]Department of Medicine, The University of Hong Kong, Hong Kong, China
[3]Department of Pharmacy and Pharmacology, The University of Hong Kong, Hong Kong, China
[4]Department of Pharmacology, Weill Cornell Medical College in Qatar, Doha, Qatar
[5]School of Biomedical Sciences, Institute of Vascular Medicine, Li Ka Shing Institute of Health Sciences, Chinese University of Hong Kong, Hong Kong, China
[6]School of Pharmaceutical Science, Wenzhou Medical University, Wenzhou, China
[7]Lead Contact
*Correspondence: zhuofenglin@wzmc.edu.cn (Z.L.), amxu@hku.hk (A.X.)
https://doi.org/10.1016/j.celrep.2019.02.014

SUMMARY

Exercise promotes adipose remodeling and improves obesity-induced metabolic disorders through mechanisms that remain obscure. Here, we identify the FGF21 signaling in adipose tissues as an obligatory molecular transducer of exercise conferring its metabolic benefits in mice. Long-term high fat diet-fed obese mice exhibit compromised effects of exogenous FGF21 on alleviation of hyperglycemia, hyperinsulinemia, and hyperlipidemia, accompanied with markedly reduced expression of FGF receptor-1 (FGFR1) and β-Klotho (KLB) in adipose tissues. These impairments in obese mice are reversed by treadmill exercise. Mice lacking adipose KLB are refractory to exercise-induced alleviation of insulin resistance, glucose dysregulation, and ectopic lipid accumulation due to diminished adiponectin production, excessive fatty acid release, and enhanced adipose inflammation. Mechanistically, exercise induces the adipose expression of FGFR1 and KLB via peroxisome proliferator-activated receptor-gamma-mediated transcriptional activation. Thus, exercise sensitizes FGF21 actions in adipose tissues, which in turn sends humoral signals to coordinate multi-organ crosstalk for maintaining metabolic homeostasis.

INTRODUCTION

Fibroblast growth factor-21 (FGF21) is an endocrine member of the FGF superfamily critically involved in the regulation of energy homeostasis, glucose and lipid metabolism, and insulin sensitivity. Physiologically, FGF21 acts as a stress-responsive hormone induced by a variety of cellular stressors such as starvation and cold challenge, which in turn facilitates the adaptation to the stress environment by promoting gluconeogenesis, ketogenesis, and adaptive thermogenesis (Fisher et al., 2012; Inagaki et al., 2007; Liang et al., 2014). Pharmacologically, administration of recombinant FGF21 protein has been shown to correct obesity and its related metabolic disorders in both rodents and non-human primates (Coskun et al., 2008; Kharitonenkov et al., 2007). In patients with obesity and type 2 diabetes, chronic administration of FGF21 analogs produces significant improvements in dyslipidemia and modest reduction in body weight and insulin resistance, but has minimal benefits on hyperglycemia (Gaich et al., 2013; Talukdar et al., 2016). Paradoxically, despite its multiple therapeutic benefits, circulating FGF21 was elevated in obese subjects (Zhang et al., 2008) and was an independent predictor for a cluster of cardiometabolic diseases (Chen et al., 2011a; Chow et al., 2013; Li et al., 2013).

FGF21 utilizes the conventional FGF receptor-1 (FGFR1) and the co-receptor β-Klotho (KLB) in cell surface to initiate the intracellular signaling cascades in its target tissues, including brain, adipose tissues, and pancreas (Fon Tacer et al., 2010; Ming et al., 2012). In particular, adipose tissues, where both FGFR1 and KLB are abundantly expressed, are critical targets mediating pleiotropic metabolic effects of FGF21 (Luo and McKeehan, 2013). In adipocytes, FGF21 promotes insulin-independent glucose uptake, regulates lipolysis, induces adiponectin secretion, and increases mitochondrial biogenesis (Fisher et al., 2012; Ge et al., 2011; Lin et al., 2013; Park et al., 2016). Both fatless mice and mice with adipocyte-specific deletion of *FGFR1* or *KLB* are resistant to the therapeutic benefits of FGF21 administration on insulin sensitivity, glucose tolerance, and lipid homeostasis (Adams et al., 2012; Ding et al., 2012; Véniant et al., 2012). Expression of the FGF21 receptor complex, especially KLB, is repressed in adipose tissues of dietary obese mice as well as obese humans (Li et al., 2018), which may account for FGF21 resistance observed in several animal-based studies (Fisher et al., 2010; Ge et al., 2011). Indeed, transgenic overexpression of KLB in adipose tissue is sufficient to enhance FGF21 response and combat dietary obesity in mice (Samms et al., 2016).

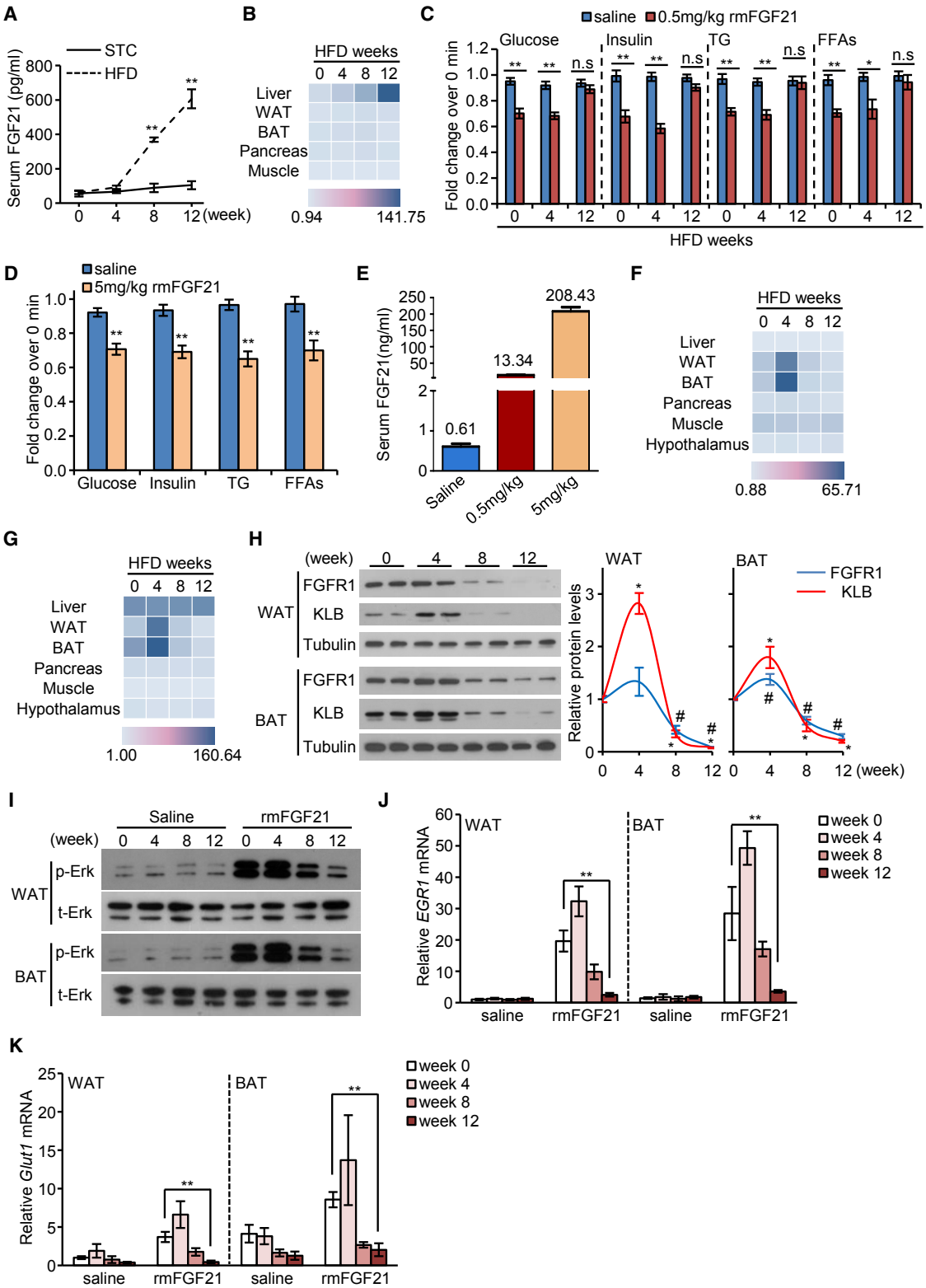

Figure 1. Dynamic Changes in Circulating FGF21, Expression of FGF21 Receptors, and FGF21 Sensitivity in Dietary Obese Mice

10-week-old male C57BL/6J mice were fed with standard chow (STC) or high fat diet (HFD) for 0, 4, 8, and 12 weeks as specified.

(A) Serum FGF21 levels measured by ELISA (n = 7–9, **p < 0.01 versus STC at the same time point).

(legend continued on next page)

Regular exercise is a non-pharmacological polypill for prevention and treatment of obesity-related cardiometabolic diseases through modulation of metabolism and function of multiple organs, including skeletal muscle, adipose tissue, brain, and heart (Boström et al., 2013). In adipose tissue, exercise training reduces lipid content and inflammation, regulates browning and thermogenesis, as well as modulates production of adipokines (Görgens et al., 2015; Stanford et al., 2015a; Thompson et al., 2012). However, how exercise causes such adipose remodeling and whether or not adipose actions of exercise contribute to systemic improvement of insulin sensitivity and glucose homeostasis remain undetermined. FGF21 has been identified as an exercise-responsive factor in both rodents and humans. Circulating FGF21 is elevated by both maximal and submaximal acute exercise in lean subjects (Kim et al., 2013) but is reduced after long-term exercise in obese or elderly individuals (Taniguchi et al., 2016; Yang et al., 2011), as well as in obese rodents (Fletcher et al., 2012). Given that adipose tissue is an important target of FGF21, we investigated whether FGF21 signaling mediates the adipose remodeling of exercise, and whether adipose actions of FGF21 confer the systemic effects of exercise on glucose and lipid metabolism and insulin sensitivity in mice.

RESULTS

Long-Term HFD Leads to FGF21 Resistance in Adipose Tissues

Consistent with previous studies (Fisher et al., 2010; Hale et al., 2012), the serum levels of FGF21 in C57BL/6J mice were gradually increased in response to high fat diet (HFD). Although there was no significant difference between HFD- and standard chow (STC)-fed groups at 4 weeks, serum levels of FGF21 were ~6-fold higher than STC-fed mice after 12 weeks of HFD feeding (Figure 1A). Similarly, mice fed with HFD exhibited a progressively increased *FGF21* mRNA expression in the liver (Figure 1B; Table S1), which is the primary organ for production of circulating FGF21 (Markan et al., 2014). To evaluate FGF21 sensitivities at different stages of dietary obesity *in vivo*, age-matched mice fed with HFD for 0, 4, and 12 weeks were treated with recombinant mouse FGF21 (rmFGF21) protein (0.5 mg/kg body weight) or saline by intraperitoneal injection. In mice fed with HFD for 0 and 4 weeks, administration of rmFGF21 significantly lowered blood glucose and serum levels of insulin, triglycerides (TG), and free fatty acids (FFAs) (Figure 1C; Table S2), whereas such effects of rmFGF21 were largely compromised in mice fed with HFD for 12 weeks. An obvious pharmacological response in 12-week HFD-fed mice was observed when the dose of rmFGF21 was increased to 5 mg/kg body weight (Figure 1D; Table S3), which resulted in an ~15-fold elevation of serum FGF21 concentrations than dose of 0.5 mg/kg (Figure 1E), suggesting that long-term dietary obesity blunts FGF21 sensitivity and causes FGF21 resistance, whereas the maximal responsiveness remains intact.

FGF21 exerts its metabolic actions by binding to a receptor complex between FGFR1 and KLB (Lee et al., 2018; Ming et al., 2012). We next analyzed the expression patterns of FGFR1 and KLB in several major target tissues of FGF21 during the development of dietary obesity. Surprisingly, 4-week HFD feeding upregulated mRNA and protein levels of FGFR1 and KLB in epididymal white adipose tissue (WAT), subcutaneous WAT (data not shown), and brown adipose tissue (BAT), whereas prolonged HFD feeding for 12 weeks markedly suppressed the expression of both FGFR1 and KLB in these adipose depots (Figures 1F–1H; Table S1). Expression of *FGFR1* or *KLB* in other FGF21 target tissues, including liver, pancreas, skeletal muscle, and hypothalamus, did not show significant changes during either short-term or long-term HFD feeding (Figures 1F and 1G; Table S1), suggesting that adipose tissues are perhaps the main organ contributing to FGF21 resistance caused by chronic HFD. Indeed, FGF21-elicited post-receptor signaling events in adipose tissues, including phosphorylation of the MAP kinase Erk1/2 (Thr202/Tyr204), and expression of the transcription factor early growth response 1 (*EGR1*) and glucose transporter 1 (*Glut1*), were abrogated in mice fed with HFD for 12 weeks, but

(B) Heatmap represents the relative *FGF21* mRNA expression levels in liver, epididymal WAT, BAT, pancreas, and gastrocnemius muscle collected at different time intervals under HFD challenge and measured by real-time PCR (see color scale). The absolute mean and SEM value of each group are provided in Table S1 (n = 5).

(C) 0.5 mg/kg body weight of rmFGF21 or saline was intraperitoneally (i.p.) injected into age-matched mice on HFD for 0, 4, and 12 weeks. Blood glucose and serum levels of insulin, TG, and FFAs were measured at 180 min, 120 min, 120 min, and 90 min after injection, respectively. Fold change over basal level (0 min) was calculated (n = 6-7). The absolute mean ± SEM values of each group are provided in Table S2. n.s., not significant.

(D) Mice fed with HFD for 12 weeks were i.p. injected with 5 mg/kg body weight of rmFGF21 or saline. Blood glucose and serum levels of insulin, TG, and FFAs were measured at 180 min, 120 min, 120 min, and 90 min after injection, respectively. Fold change over basal level (0 min) was calculated (n = 6–7). The absolute mean ± SEM values of each group are provided in Table S3.

(E) Mice fed with HFD for 12 weeks were i.p. injected with saline, 0.5 mg/kg, or 5 mg/kg body weight of rmFGF21 protein. Serum FGF21 levels were measured by ELISA at 90 min after injection (n = 6–7).

(F and G) Heatmap represents the relative *FGFR1* (F) and *KLB* (G) mRNA expression levels in liver, epididymal WAT, BAT, pancreas, gastrocnemius muscle, and hypothalamus collected at different time intervals under HFD challenge and measured by real-time PCR (see color scale). The mean value and SEM value of each group are provided in Table S1 (n = 5).

(H) Representative immunoblotting for FGFR1 and KLB in epididymal WAT and BAT collected at different time intervals under HFD challenge and quantification by normalization to tubulin after densitometric quantification of protein bands (n = 4, #$p < 0.05$, compared with FGFR1 level at week 0; *$p < 0.05$, compared with KLB level at week 0).

(I–K) 0.5 mg/kg body weight of rmFGF21 or saline was i.p. injected into age-matched mice on HFD for 0, 4, 8, and 12 weeks. Adipose tissues were collected at 10 min after injection and subjected to immunoblotting analysis for total or phosphorylated Erk (Thr202/Tyr204) (I), or collected at 90 min after injection and subjected to real-time PCR analysis for quantification of *EGR1* mRNA levels (J), or collected at 6 h after injection and subjected to real-time PCR analysis for quantification of *Glut1* mRNA levels (K) (n = 5).

Data are represented as mean ± SEM, *$p < 0.05$, **$p < 0.01$. Representative data from three independent experiments are shown.

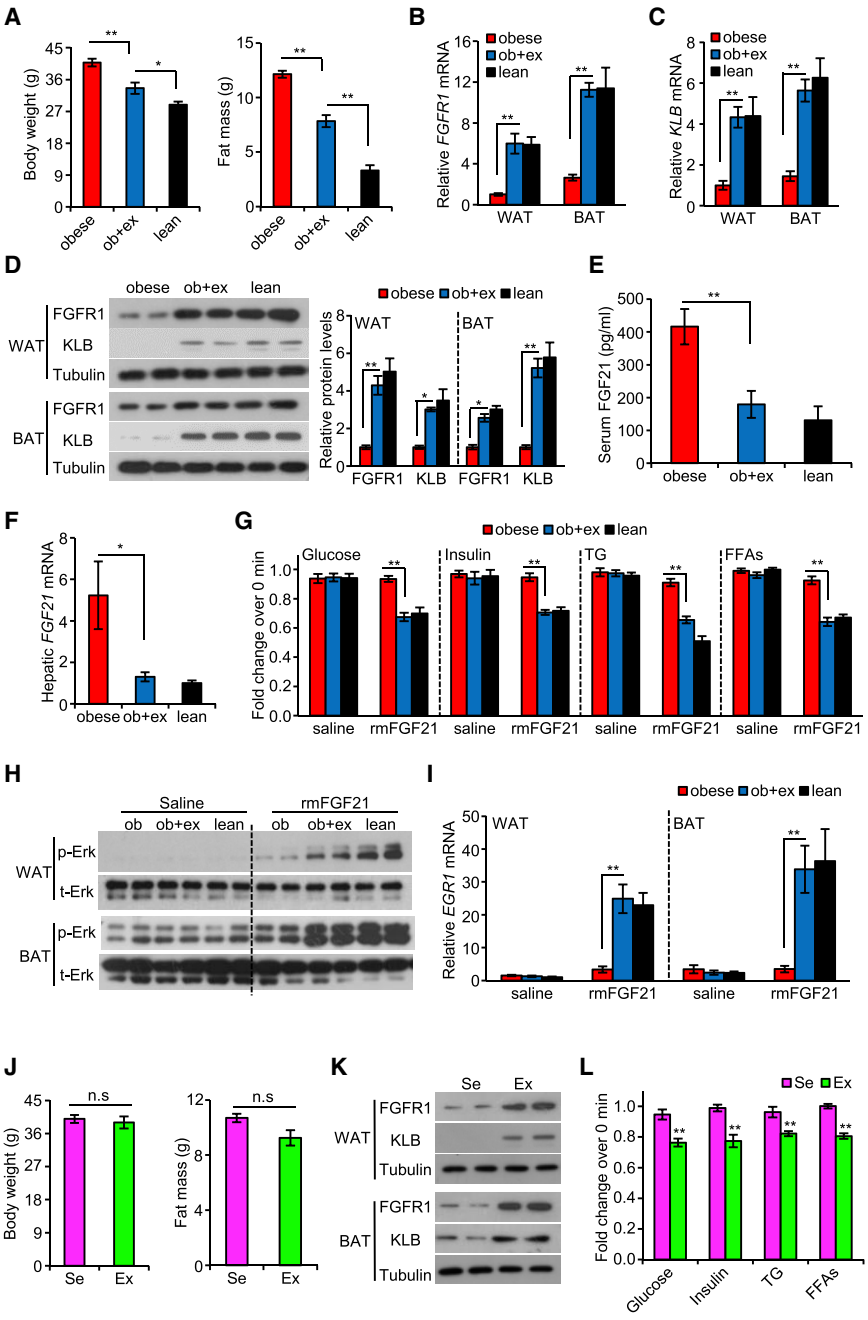

Figure 2. Exercise Induces Expression of the FGF21 Receptor Complexes in Adipose Tissues and Attenuates Diet-Induced FGF21 Resistance in Obese Mice

For (A)–(I), 10-week-old male C57BL/6J mice were fed with STC or HFD for 12 weeks as lean or obese groups respectively. The exercised obese (ob+ex) mice were subjected to treadmill running at the last 4 weeks during total 12-week-HFD feeding. For (J)–(L), 10-week-old male C57BL/6J mice fed with HFD for 12 weeks were divided into two groups, sedentary group (Se) and exercised group (Ex). The exercised mice received 3-day treadmill training.

(A) Body weight and fat mass monitored using a rodent body composition analyzer (n = 6–7).

(B and C) The relative mRNA levels of *FGFR1* (B) and *KLB* (C) in epididymal WAT and BAT measured by real-time PCR and normalized to *β-actin* gene (n = 5).

(D) Representative immunoblotting for FGFR1 and KLB in epididymal WAT and BAT (left) and quantification of their relative expression levels with densitometry (right) (n = 6). Tubulin, internal control.

(E) Serum FGF21 levels measured by ELISA (n = 8–12).

(F) Hepatic *FGF21* mRNA levels measured by real-time PCR and normalized to *β-actin* gene (n = 6).

(G) Mice were i.p. injected with 0.5 mg/kg body weight of rmFGF21 or saline. Blood glucose and serum levels of insulin, TG, and FFAs were measured at 180 min, 120 min, 120 min, and 90 min after injection, respectively. Fold change over basal level (0 min) was calculated (n = 5–6). The absolute mean ± SEM values of each group are provided in Table S4.

(H and I) 0.5 mg/kg body weight of rmFGF21 or saline was i.p. injected into mice. Adipose tissues were collected at 10 min after injection and subjected to immunoblotting analysis for total or phosphorylated Erk (Thr202/Tyr204) (H), or collected at 90 min after injection and subjected to real-time PCR analysis for quantification of *EGR1* mRNA levels (I) (n = 5).

(J) Body weight and fat mass monitored using a rodent body composition analyzer (n = 5). n.s., not significant.

(K) Representative immunoblotting for FGFR1 and KLB in epididymal WAT and BAT. Tubulin, internal control.

(L) Mice were i.p. injected with 0.5 mg/kg body weight of rmFGF21. Blood glucose and serum levels of insulin, TG, and FFAs were measured at 180 min, 120 min, 120 min, and 90 min after injection, respectively. Fold change over basal level (0 min) was calculated (n = 5). The absolute mean ± SEM values of each group are provided in Table S5.

Data are represented as mean ± SEM, *p < 0.05, **p < 0.01. Representative data from three independent experiments are shown. See also Figure S1.

not for 4 weeks (Figures 1I–1K). Collectively, long-term HFD challenge leads to selective FGF21 resistance in adipose tissues of mice.

Exercise Reverses Long-Term HFD-Induced FGF21 Resistance Independent of Adiposity

FGF21 has been proposed as an important mediator for physical exercise-induced metabolic benefits in mice (Loyd et al., 2016). Therefore, we next investigated whether exercise can reverse FGF21 resistance associated with dietary obesity. To this end, male C57BL/6J mice on HFD for 8 weeks were subjected to treadmill training for another 4 weeks. The body weight and fat mass in the exercised mice were reduced by 17.7% and 35.4%, respectively, compared to HFD fed-mice with sedentary lifestyle but remained much higher than age-matched lean mice fed with STC (Figure 2A). On the other hand, 4-week treadmill

exercise led to a marked reversal of HFD-induced downregulation of FGFR1 and KLB in both WAT and BAT (Figures 2B–2D), whereas it had no obvious effects on several other FGF21 target tissues examined (Figures S1A and S1B). In parallel, HFD-induced elevations of both circulating levels of FGF21 and hepatic *FGF21* mRNA expression were markedly reduced by exercise training to levels comparable to STD-fed lean mice (Figures 2E and 2F). In response to a single injection of rmFGF21 protein (0.5 mg/kg body weight), exercised obese mice exhibited much greater reductions in blood glucose levels and serum levels of insulin, TG, and FFAs compared to sedentary obese mice (Figure 2G; Table S4). Furthermore, the induction of Erk1/2 phosphorylation and *EGR1* expression in adipose tissues of exercise-trained mice by rmFGF21 was significantly stronger than in sedentary obese mice (Figures 2H and 2I).

To further exclude the possibility that the improvement in FGF21 sensitivity of exercised mice is secondary to the body weight reduction, we also tested the effects of rmFGF21 in HFD-fed obese mice receiving short-term treadmill training (3 days), which had no obvious effects on body weight or fat mass (Figure 2J). Notably, 3 days of treadmill exercise was sufficient to upregulate the expression of both FGFR1 and KLB in WAT and BAT (Figure 2K), accompanied by significantly improved metabolic benefits of rmFGF21 on glucose and lipid metabolism compared to sedentary obese mice (Figure 2L; Table S5), suggesting that both long-term and short-term exercise can alleviate obesity-induced FGF21 resistance by upregulating adipose FGFR1 and KLB, independent of changes in adiposity.

Adipose Actions of FGF21 Are Obligatory in Mediating the Metabolic Benefits of Exercise on Systemic Insulin Sensitivity and Glucose Homeostasis

The tissue specificity of FGF21 is determined by its co-receptor KLB, a single transmembrane glycoprotein, which is highly expressed in adipose tissues (Kurosu et al., 2007). To investigate whether upregulated adipose KLB mediates the systemic benefits of exercise, we generated adipocyte-specific KLB knockout (Klb^{adi}) mice by crossing *loxP*-flanked $Klb^{f/f}$ mice with adiponectin-cre transgenic mice in C57BL/6J background (Huang et al., 2017; Li et al., 2018). Consistent with a previous study (Ding et al., 2012), Klb^{adi} mice grew normally and showed a comparable body weight, fat mass, blood glucose level, and insulin sensitivity with $Klb^{f/f}$ littermates on both STC and HFD (Figures S2A–S2D). 4-week treadmill exercise training significantly reduced HFD-induced elevation of body weight to a similar extent between $Klb^{f/f}$ and Klb^{adi} mice (Figure 3A), but the exercised Klb^{adi} mice had less weight of epididymal WAT but more liver weight than exercised $Klb^{f/f}$ mice (Figure 3B). Exercise increased energy expenditure and food intake in both $Klb^{f/f}$ and Klb^{adi} mice, but there were no obvious differences between the two groups (Figures S3A–S3C). In line with a previous study (Ding et al., 2012), there were no obvious differences in glucose excursions during glucose tolerance test (GTT) and insulin tolerance test (ITT) between the two groups of HFD-fed mice without exercise training (Figures 3C and 3D). As expected, treadmill exercise for 4 weeks markedly alleviated HFD-induced glucose intolerance, insulin resistance, and hyperinsulinemia in $Klb^{f/f}$ mice, whereas such effects of exercise were significantly attenuated in Klb^{adi} mice (Figures 3C–3E). Likewise, the effects of treadmill exercise on reduction of circulating TG and FFAs were largely compromised in Klb^{adi} mice compared to $Klb^{f/f}$ mice (Figures 3F and 3G). Furthermore, exercise-induced reduction of serum FGF21 levels (Figure 3H) and its hepatic mRNA expression (Figure 3I) were significantly compromised in Klb^{adi} mice. In summary, mice lacking adipose KLB were refractory to exercise-induced improvements of glycemic control and lipid homeostasis.

To further test whether FGF21 signaling is obligatory for exercise-induced metabolic benefits, we also compared the effects of treadmill exercise between FGF21 knockout ($FGF21^{-/-}$) mice and their wild-type ($FGF21^{+/+}$) littermates. Similar to the results observed from Klb^{adi} mice, $FGF21^{-/-}$ mice had similar body weights, less epididymal WAT weight, but more liver weight than $FGF21^{+/+}$ mice after exercise training (Figures S4A and S4B). Expectedly, the beneficial effects of exercise on attenuation of glucose intolerance, insulin resistance, and hyperinsulinemia were significantly compromised in $FGF21^{-/-}$ mice (Figures S4C–S4E). Furthermore, lack of FGF21 weakened the effects of exercise on lowering circulating TG and FFAs levels in dietary obese mice (Figures S4F and S4G).

FGF21 Mediates Exercise-Induced Alleviation of Obesity-Induced Ectopic Lipid Accumulation and Insulin Insensitivity in Non-adipose Organs by Adipose Remodeling

To investigate how FGF21 acts on adipose tissues to regulate whole body glucose and lipid homeostasis during exercise, we next compared histological and molecular changes between HFD-fed dietary obese Klb^{adi} mice and $Klb^{f/f}$ mice in response to treadmill training. Consistent with the changes in liver weight (Figure 3B), exercise-induced reduction of hepatic lipid deposition was observed in both genotypes. However, the exercised $Klb^{f/f}$ mice exhibited much greater degree of reduction in hepatic steatosis and hepatic levels of TG and FFAs than those exercised Klb^{adi} mice (Figures 4A–4C). Likewise, exercise-induced decrease of lipid accumulation in skeletal muscle of Klb^{adi} mice was significantly compromised as compared to $Klb^{f/f}$ mice (Figures 4B and 4C). Furthermore, exercise-induced fatty acid oxidation (FAO) and the expression of genes related with fatty acids β-oxidation were reduced in liver and skeletal muscle of Klb^{adi} mice compared with their $Klb^{f/f}$ littermates (Figures 4D and 4E).

Similar to Klb^{adi} mice, exercised $FGF21^{-/-}$ mice also showed higher lipid contents and lower FAO capacities in the liver and skeletal muscle than exercised wild-type littermates (Figures S5A–S5C). Biochemical analysis showed that the magnitude of exercise-induced alleviation in liver injury, as estimated by serum alanine aminotransferase (ALT) levels was also reduced in Klb^{adi} or $FGF21^{-/-}$ mice compared to their respective wild-type controls (Figures 4F and S5F). Additionally, both Klb^{adi} and $FGF21^{-/-}$ mice were partially resistant to chronic exercise-induced mitochondrial biogenesis in skeletal muscle, as evidenced by reduced mitochondrial DNA content (Figures 4G and S5G) and expression of genes related with mitochondrial biogenesis after exercise intervention (Figures 4H and S5H). Expectedly, exercise-induced improvement of insulin sensitivity was compromised in the liver and gastrocnemius muscle of mice lacking FGF21 actions in adipose tissues, as demonstrated by

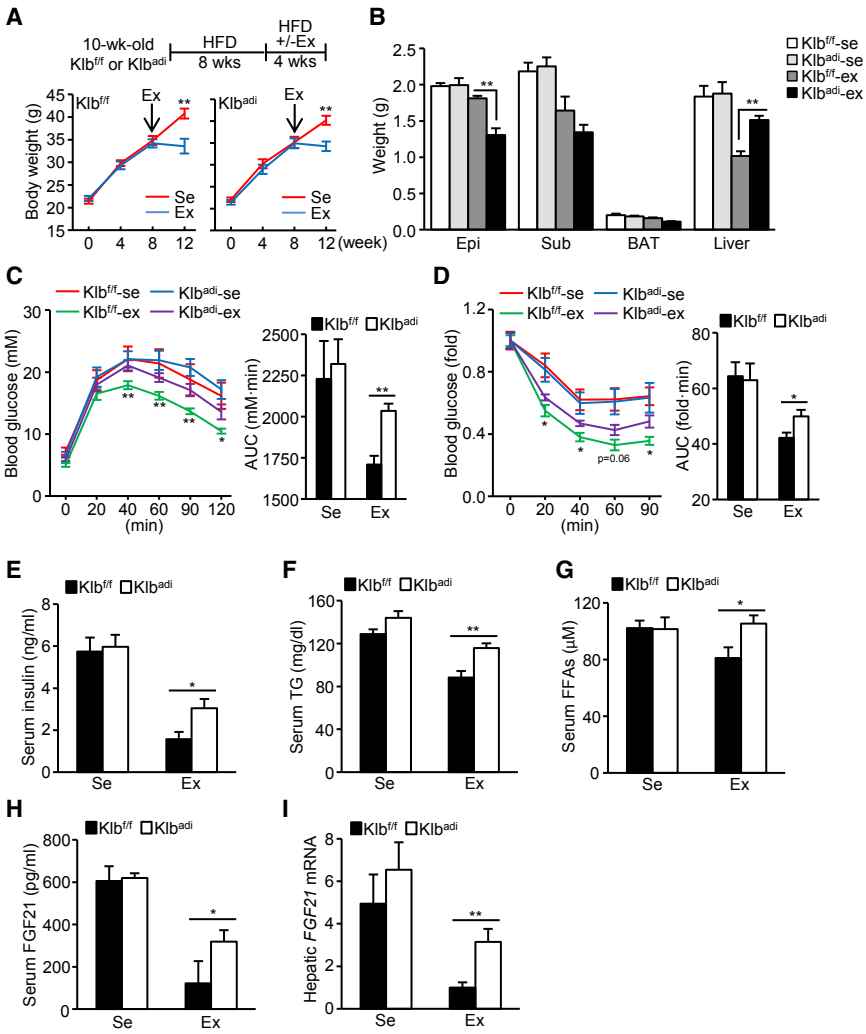

Figure 3. Mice with Adipocyte-Specific Ablation of KLB Are Refractory to Exercise-Induced Improvements of Glycemic Control and Lipid Homeostasis

10-week-old male Klb$^{f/f}$ and Klb^{adi} mice were fed with HFD for 12 weeks. The mice were either subjected to treadmill running (Ex) or sedentary lifestyle (Se) at the last 4 weeks during total 12-week-HFD feeding.

(A) Schematic representation of experimental design (top) and dynamic changes of body weight of Klb$^{f/f}$ and Klb^{adi} mice during the whole experiments (bottom) (n = 7–11,**p < 0.01 compared with exercised mice of the same genotype).

(B) Wet weights of epididymal WAT (Epi), subcutaneous WAT (Sub), BAT, and liver (n = 7–10).

(C) GTT performed at the third week of exercise training and area under curve (AUC) during GTT (n = 7–11, *Klb$^{f/f}$-ex versus Klb^{adi}-ex).

(D) ITT performed at the last week of exercise training and AUC during ITT (n = 7–9, *Klb$^{f/f}$-ex versus Klb^{adi}-ex).

(E) Serum fasting insulin levels measured by ELISA at the end of experiment (n = 7).

(F and G) Serum fasting triglyceride (TG) (F) and free fatty acids (FFAs) (G) levels measured by biochemical analysis at the end of experiment (n = 7–11).

(H) Serum feeding FGF21 levels measured by ELISA at the end of experiment (n = 7).

(I) Hepatic *FGF21* mRNA levels measured by real-time PCR and normalized to *β-actin* gene (n = 6).

Data are represented as mean ± SEM, *p < 0.05, **p < 0.01. Representative data from three independent experiments are shown. See also Figures S2–S4.

Akt phosphorylation (Ser473) after insulin stimulation (Figures 4I and 4J). Taken together, these findings suggest that the metabolic benefits of exercise in non-adipose organs, including liver and skeletal muscle, are mediated, at least in part, by FGF21 actions in adipose tissues.

We next interrogated how adipose actions of FGF21 lead to increased FAO and decreased lipid accumulation in distal organs after exercise intervention. First, given the critical roles of adiponectin in promoting FAO of liver and skeletal muscle (Yamauchi et al., 2002), and in mediating the therapeutic benefits of FGF21 in distant organs (Holland et al., 2013; Lin et al., 2013), we hypothesized that adiponectin is one of the potential mediators. In line with previous studies (Garekani et al., 2011; Kriketos et al., 2004), chronic exercise led to a significant elevation in serum adiponectin levels and adiponectin expression in adipose tissue of both Klb$^{f/f}$ and Klb^{adi} mice (Figures 5A and 5B). However, the degree of exercise-induced elevation of adiponectin expression and its circulating concentration in Klb^{adi} mice was much smaller than those in Klb$^{f/f}$ mice (Figures 5A and 5B). Likewise, we also observed that exercised FGF21$^{-/-}$ mice had lower adiponectin levels in both circulation and local adipose depot when compared with exercised FGF21$^{+/+}$ mice (Figures S5I and S5J).

Second, considering FGF21 inhibits adipose lipolysis and reduces FFAs influx to non-adipose organs (Arner et al., 2008; Chen et al., 2011b; Li et al., 2009), we next investigated whether such adipose actions of FGF21 contribute to the beneficial effects of exercise on depletion of ectopic lipid accumulation. Consistent with less wet weight of epididymal WAT after exercise (Figure 3B), the exercised Klb^{adi} mice had much smaller white adipocytes than the exercised Klb$^{f/f}$ mice (Figure 5C), accompanied by significantly higher lipolytic activities (Figure 5D) due to a greater degree of increased adipose TG lipase (ATGL) and phosphorylation of hormone-sensitive lipase (HSL, Ser660) after exercise intervention (Figure 5E). Similar to Klb^{adi} mice, exercised FGF21$^{-/-}$ mice also had smaller white adipocytes, higher lipolytic activities and more lipolytic enzymes in epididymal WAT than those of exercised wild-type littermates (Figures S5K–S5M), suggesting that the lack of FGF21 actions in adipose tissues may exacerbate exercise-induced lipolysis and adipose-derived FFAs influx to liver and skeletal muscle.

Third, given the suppressive effect of FGF21 on adipose tissue-derived inflammatory factors (Asrih et al., 2015; Li et al.,

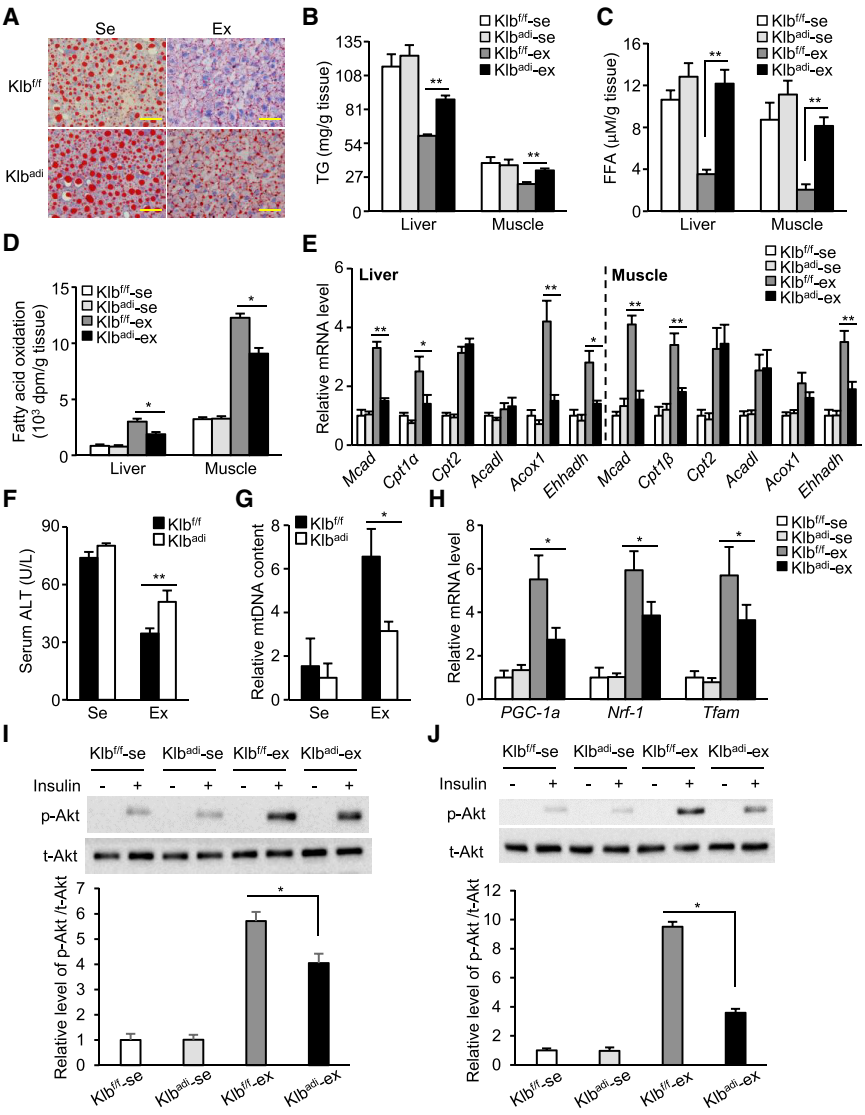

Figure 4. Mice with Adipocyte-Specific Ablation of KLB Are Resistant to Exercise-Induced Alleviation of Ectopic Lipid Accumulation and Insulin Resistance in Non-adipose Organs

10-week-old male $Klb^{f/f}$ and Klb^{adi} mice fed with HFD were subjected to sedentary lifestyle (Se) or treadmill exercise (Ex) for 4 weeks as described in Figure 3.

(A) Oil Red O staining of liver sections. Scale bars, 50 μm.

(B and C) Triglyceride (TG) (B) and FFAs (C) levels in liver and gastrocnemius muscle (n = 6).

(D) Fatty acids oxidation (FAO) capacity in liver and gastrocnemius muscle as measured with ^{14}C-labeled palmitic acid oxidation assay (n = 6).

(E) The mRNA expression levels of fatty acids β-oxidation-related genes (*Mcad*, medium-chain acyl-CoA dehydrogenase; *Cpt1/2*, carnitine palmitoyltransferase 1/2; *Acadl*, acyl-CoA dehydrogenase, long chain; *Acox1*, acyl-CoA oxidase 1; *Ehhadh*, enoyl-CoA hydratase, and 3-hydroxyacyl CoA dehydrogenase) in liver and gastrocnemius muscle, as quantified by real-time PCR and normalized to *β-actin* gene (n = 6).

(F) Serum alanine aminotransferase (ALT) levels (n = 6–8).

(G) Mitochondrial DNA (mtDNA) content in gastrocnemius muscle, as quantified by mitochondrial cytochrome B (*CytB*) gene and normalized to genomic DNA by amplification of the large ribosomal protein p0 (*36B4*) nuclear gene (n = 6).

(H) Expression levels of genes related with mitochondrial biogenesis (*PGC-1α*, peroxisome proliferator-activated receptor gamma coactivator-1 alpha; *Nrf-1*, nuclear respiratory factor-1; *Tfam*, mitochondrial transcription factor A) in gastrocnemius muscle as quantified by real-time PCR and normalized to *β-actin* gene (n = 6).

(I and J) 0.5 U/kg body weight of insulin or saline was injected via inferior vena cava. Liver and gastrocnemius muscle were collected at 15 min after injection and subjected to immunoblotting analysis for total or phosphorylated Akt (Ser473). The relative levels of p-Akt/t-Akt in liver (I) and gastrocnemius muscle (J) were quantified with densitometry (n = 4).

Data are represented as mean ± SEM, *p < 0.05, **p < 0.01. Representative data from three independent experiments are shown. See also Figure S5.

2018), which are well known to induce dysfunction of lipid metabolism and insulin resistance in distant organs (Reilly and Saltiel, 2017), we next investigated whether FGF21 signaling in adipose tissues contributes to exercise-induced alleviation of metabolic inflammation. As expected, chronic exercise led to a significant downregulation of inflammatory genes, including tumor necrosis factor alpha (*TNF-α*), monocyte chemoattractant protein-1 (*MCP-1*), interleukin (*IL*)-*1β*, and the macrophage surface marker *F4/80*, in WAT of $Klb^{f/f}$ mice (Figure 5F), accompanied with reduced serum levels of TNF-α and IL-1β (Figures 5G and 5H). However, such an effect of exercise on suppression of metabolic inflammation was significantly compromised in Klb^{adi} as well as in $FGF21^{-/-}$ mice (Figures 5F–5H and S5N–S5P). Collectively, enhanced FGF21 actions in adipose tissues on induction of adiponectin production, inhibition of FFAs efflux, and suppression of metabolic inflammation may contribute to the beneficial effects of exercise on alleviation of insulin resistance, glucose and lipid dysregulation and ectopic lipid accumulation.

Exercise-Induced Upregulation of Adipose FGFR1 and KLB Depends on PPARγ

As our data showed that exercise-induced FGF21 sensitization and metabolic benefits are attributed to upregulation of FGF21 receptor complexes, we next investigated how treadmill exercise promotes their expression in adipocytes. Previous studies demonstrated exercise training robustly activated peroxisome proliferator-activated receptor-gamma (PPARγ) in both rodents and humans, while treatment of the PPARγ agonist rosiglitazone promoted adipose expression of both FGFR1 and KLB (Díaz-Delfín et al., 2012; Petridou et al., 2007; Ruschke et al., 2010).

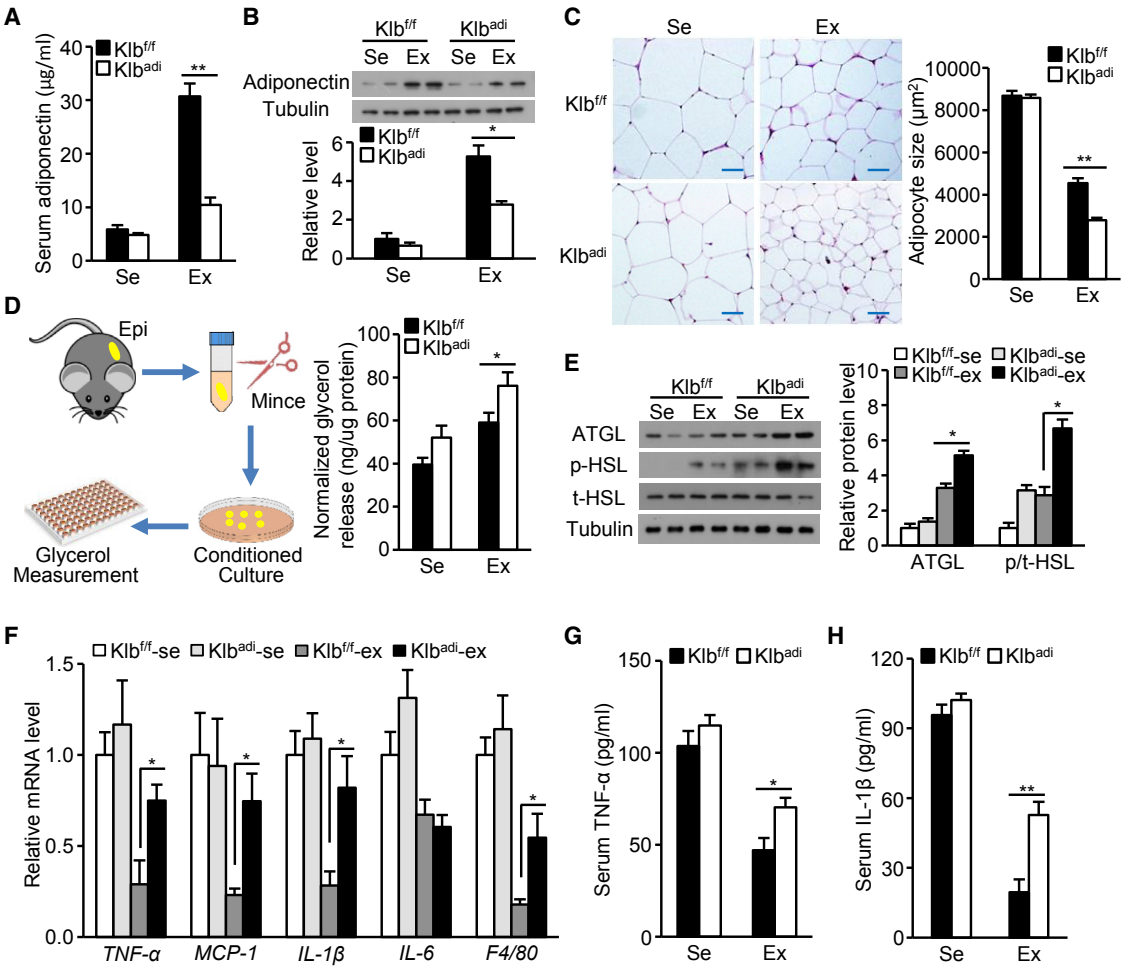

Figure 5. Exercise-Induced Adipose Remodeling Is Diminished by Adipocyte-Specific Ablation of KLB

10-week-old male $Klb^{f/f}$ and Klb^{adi} mice fed with HFD were subjected to sedentary lifestyle (Se) or treadmill exercise (Ex) for 4 weeks as described in Figure 3.

(A) Serum levels of total adiponectin measured by ELISA (n = 7).

(B) Representative immunoblotting for total adiponectin in epididymal WAT (top) and quantification of relative expression levels with densitometry (bottom) (n = 4). Tubulin, internal control.

(C) H&E staining of epididymal WAT sections (left) and quantification of average adipocyte size (right, n = 4, total 200 adipocytes were counted in each sample). Scale bars, 50 μm.

(D) Lipolytic activities of epididymal WAT (right), as measured by glycerol release from adipose explant in conditioned medium (left) (n = 6).

(E) Representative immunoblots for expression of lipolytic enzymes in epididymal WAT (top), and quantification of relative expression levels with densitometry (bottom, n = 4). Tubulin, internal control.

(F) Relative mRNA levels of inflammation-related genes (*TNF-α*, tumor necrosis factor-α; *MCP-1*, monocyte chemoattractant protein-1; *IL-1β*, interleukin-1β; *IL-6*, interleukin-6; *F4/80*, adhesion G protein-coupled receptor E1) in epididymal WAT as quantified by real-time PCR and normalized to β-*actin* gene (n = 6-8).

(G) Serum TNF-α levels measured by ELISA (n = 8).

(H) Serum IL-1β levels measured by ELISA (n = 7–8).

Data are represented as mean ± SEM, *p < 0.05, **p < 0.01. Representative data from three independent experiments are shown. See also Figure S5.

Therefore, we explored whether exercise-induced upregulation of adipose FGFR1 and KLB expression is mediated by PPARγ. Treadmill exercise for 4 weeks increased the activity of PPARγ in epididymal WAT of dietary obese mice (Figure 6A), as measured by PPARγ nuclear DNA-binding activity assay. Daily administration with GW9662 (a specific PPARγ inhibitor) for 4 weeks significantly reduced exercise-induced increase in adipose PPARγ activity (Figure 6A) and also abrogated the effects of exercise on induction of FGFR1 and KLB at both mRNA and protein levels (Figures 6B–6D). *In silico* analysis found that the proximal murine *FGFR1* promoter contains two putative PPAR-responsive elements (PPREs) located at positions −1,722 (PPRE1) and −453 (PPRE2) relative to the transcription starting site (Figure 6E) while the murine *KLB* promoter contains two potential PPREs located at positions −1,609 (PPRE1) and −1,080 (PPRE2), respectively (Figure 6F). To determine whether these potential PPREs mediate the induction of these two genes by PPARγ, we constructed the luciferase reporters driven by the

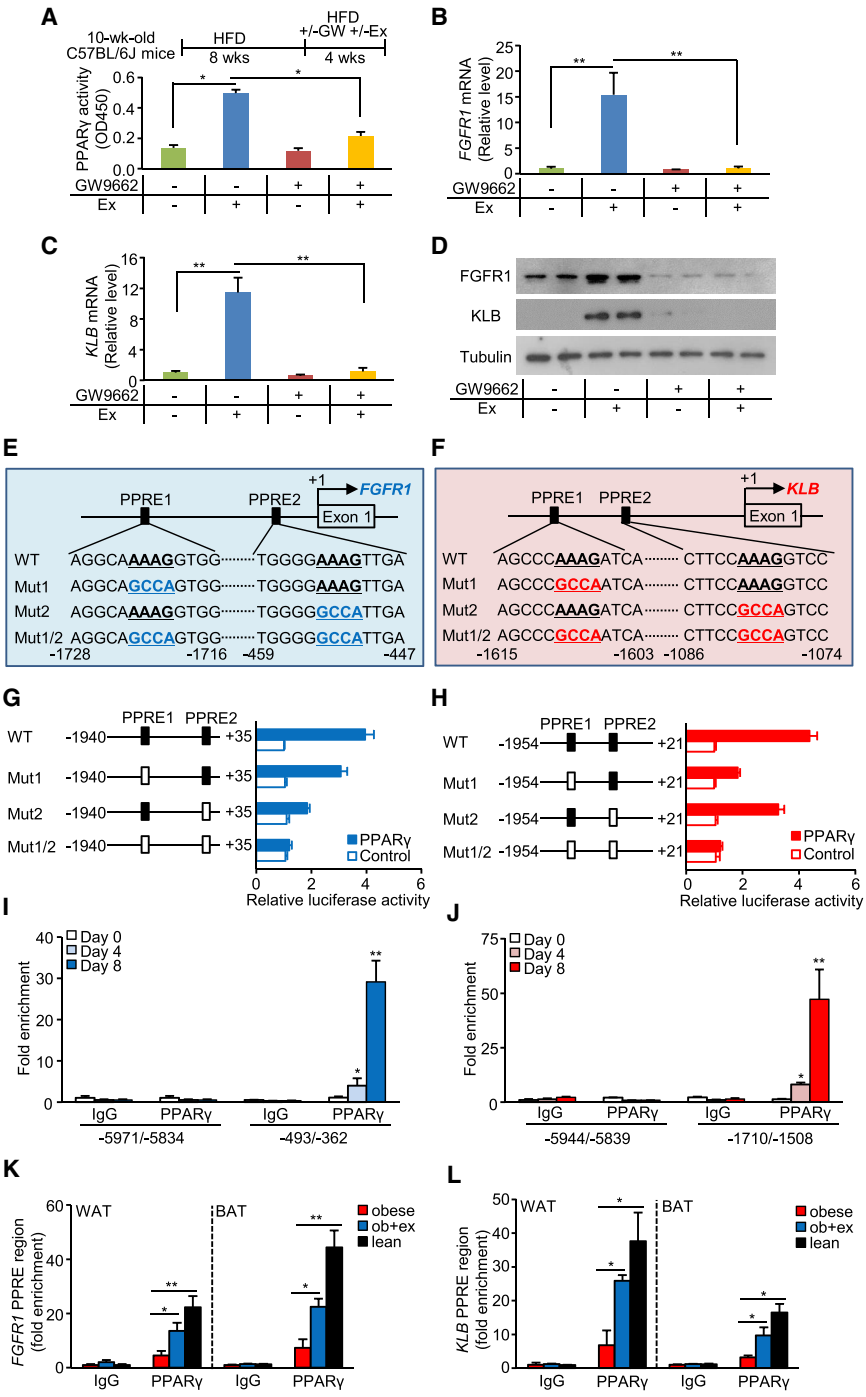

Figure 6. Exercise Induces Upregulation of FGFR1 and KLB by Activation of PPARγ in Adipose Tissue

(A) 10-week-old male C57BL/6J mice were fed with HFD for 8 weeks, and were then treated with 10 mg/kg body weight of GW9662 or vehicle (1% methylcellulose) by daily oral gavage, with or without treadmill exercise training (Ex) (top). PPARγ DNA binding activities in epididymal WAT were measured after 4 weeks of treatment (bottom) (n = 6).

(B and C) Relative mRNA expression levels of *FGFR1* (B) and *KLB* (C) in epididymal WAT measured by real-time PCR and normalized to *β-actin* gene (n = 6).

(D) Representative immunoblots for FGFR1 and KLB in epididymal WAT. Tubulin, internal control.

(E and F) Schematic diagram showing locations of two predicted PPARγ response elements (PPREs) within the 5′ flanking regions of murine *FGFR1* (E) and *KLB* (F) gene as identified by *in silico* analysis with MatInspector software and Dragon PPRE Spotter v.2.0. The site-directed mutation points were highlighted in blue and red, respectively.

(G and H) Cell-based luciferase reporter assays were performed in HEK293 cells co-transfected with luciferase-expressing vectors driven by the *FGFR1* (−1,940/+35) promoter (G) or the *KLB* promoter (−1,954/+21) (H), or the mutant promoters in which one or two PPREs were mutated, together with PPARγ expression plasmid or empty plasmid as control for 48 h. The firefly luciferase activity was measured and normalized to Renilla luciferase activity (n = 6).

(I and J) 3T3-L1 cells at different days (0, 4, or 8) after induction for adipogenic differentiation were subjected to chromatin immunoprecipitation (ChIP) analysis with a rabbit anti-PPARγ polyclonal antibody or non-immune rabbit IgG as control. The precipitated chromatin was analyzed by real-time PCR using primers to the *FGFR1* (I) or *KLB* (J) proximal promoter (−493/−362 for *FGFR1*, −1,710/−1508 for *KLB*) or a control region located ~6 kb upstream of this sequence (−5,971/−5,834 for *FGFR1*, −5,944/−5,839 for *KLB*), respectively (n = 4, *compared with day 0).

(K and L) ChIP assays with a rabbit PPARγ polyclonal antibody were performed in adipose tissues of obese, exercised obese, and lean mice (the same samples as described in Figure 2) using primers spanning to the *FGFR1* (K) and *KLB* (L) proximal promoters as described above. Non-immune IgG was used as control (n = 4).

Data are represented as mean ± SEM, *p < 0.05, **p < 0.01. Representative data from three independent experiments are shown. See also Figure S6.

murine *FGFR1* (−1,940/+35) and *KLB* promoter (−1,954/+21), or mutated promoters, in which one or two core motif of -AAAG- within the predicted PPREs was mutated into -GCCA- (Couture and Blouin, 2011) (Figures 6E and 6F). Overexpression of PPARγ significantly increased the promoter activities of *FGFR1* and *KLB* in HEK293 cells when compared with those transfected with empty vector as controls (Figures 6G and 6H). Mutation analysis showed that mutating PPRE2 in the *FGFR1* promoter and PPRE1 in *KLB* promoter resulted in a much greater loss of their PPARγ responses, and mutation of both PPREs completely abolished PPARγ-mediated activation of the *FGFR1* and *KLB* promoters (Figures 6G and 6H).

To determine whether PPARγ binds to the *FGFR1* or *KLB* promoter in adipocyte, chromatin immunoprecipitation assays were

performed in 3T3-L1 cells under adipogenic differentiation for different days. The binding of PPARγ to the PPRE region of *FGFR1* promoter (−493/−362) and *KLB* promoter (−1,710/−1,508) were gradually increased during adipogenic differentiation of 3T3-L1 cells, but not in the control regions (−5,971/−5,834 for *FGFR1*, −5,944/−5,839 for *KLB*) (Figures 6I and 6J). Additionally, chronic exercise significantly reversed HFD-induced reduction in PPARγ binding to the PPRE-containing promoter regions of both *FGFR1* and *KLB* in epididymal WAT (Figures 6K and 6L). Taken together, these results suggest that chronic exercise-induced upregulation of adipose *FGFR1* and *KLB* is mediated by PPARγ.

In addition, because FGF21 also promotes PPARγ activity in adipocytes (Dutchak et al., 2012; Lin et al., 2013), it suggests a positive feedback loop between FGF21-PPARγ-FGFR1/KLB upon chronic exercise. Indeed, in our exercised model, both FGF21$^{-/-}$ and Klb^{adi} mice were refractory to chronic exercise-induced upregulation of PPARγ activity when compared with wild-type (WT) mice (Figures S6A and S6B).

Rosiglitazone Mimics the Effects of Exercise to Reduce FGF21 Resistance in Obese Mice

Given that PPARγ mediates exercise-induced expression of the FGF21 receptor complexes in adipose tissue, we next investigated whether rosiglitazone could mimic the metabolic benefits of exercise by enhancing FGF21 sensitivity in dietary obese mice. Consistent with a previous study (Díaz-Delfín et al., 2012), administration of rosiglitazone effectively reversed HFD-reduced mRNA and protein levels of FGFR1 and KLB in adipose tissues (Figures 7A–7C). In parallel, both the serum FGF21 levels and hepatic *FGF21* mRNA levels were decreased by rosiglitazone treatment (Figures 7D and 7E). Notably, the impaired responses of dietary obese mice to a single bout of rmFGF21 (0.5 mg/kg body weight), including reductions in blood glucose and serum levels of insulin, TG, and FFAs, were all restored by rosiglitazone treatment to a level comparable to lean mice (Figure 7F; Table S6). Furthermore, rosiglitazone treatment also restored the sensitivity of FGF21 in induction of phosphorylation of Erk and *EGR1* expression in adipose tissues (Figures 7G and 7H), suggesting that the PPARγ agonist has similar FGF21-sensitizing effects as exercise by induction of adipose FGFR1 and KLB.

To further examine whether rosiglitazone exerts its metabolic benefits by enhancing FGF21 signaling in adipose tissues, we compared the effects of rosiglitazone treatment in Klb$^{f/f}$ and Klb^{adi} mice with dietary obesity. In line with previous studies (Díaz-Delfín et al., 2012; Dutchak et al., 2012), 2-week rosiglitazone treatment had minimal effects on body weight (Figure 7I). However, it significantly reduced glucose intolerance and insulin resistance in obese Klb$^{f/f}$ mice, whereas such therapeutic benefits of rosiglitazone were significantly compromised in obese Klb^{adi} mice, as determined by glucose and insulin tolerance tests (Figures 7J and 7K). Likewise, the effects of rosiglitazone treatment on reduction of serum insulin and elevation of circulating adiponectin in obese Klb^{adi} mice were markedly attenuated when comparing to those in obese Klb$^{f/f}$ mice (Figures 7L and 7M). Collectively, these data suggest that the metabolic benefits of rosiglitazone are mediated in part by enhancing FGF21 sensitivity in adipose tissues.

DISCUSSION

Exercise combats multiple chronic diseases, such as diabetes and cardiovascular dysfunction, through its profound effects on systemic metabolism and functions of almost all the major organs (Kujala, 2009). In adipose tissues, exercise regulates production and secretion of adipokines (Görgens et al., 2015), suppresses metabolic inflammation (Lancaster and Febbraio, 2014), and promotes lipolysis (Polak et al., 2008) and browning (Stanford et al., 2015b). However, whether such adipose remodeling contributes to the systemic effects of exercise on insulin sensitivity and metabolic homeostasis remains undefined. In this connection, our present study identifies adipose actions of FGF21 as an obligatory mediator for the systemic effects of exercise, by fine-tuning the crosstalk among adipose tissues, liver, and skeletal muscle.

Despite the multiple metabolic benefits of FGF21, its circulating levels are elevated in obesity and related cardiometabolic syndromes (Zhang et al., 2008), suggesting a state of "FGF21 resistance." Indeed, impaired FGF21 signaling cascades in white adipose tissues, including reduced Erk phosphorylation and expression of FGF21-responsive genes (*EGR1* and *c-FOS*) and compromised reduction of blood glucose following administration of low-dose FGF21, have been observed in dietary obese mice (Asrih et al., 2015; Fisher et al., 2010). Likewise, the cardioprotective effects of FGF21 are also attenuated in obese rats compared to lean controls (Patel et al., 2014). By contrast, another independent study in two different rodent models of obesity does not support the existence of FGF21 resistance, despite decreased expression of the FGF21 receptor complexes in adipose tissues (Hale et al., 2012). These discrepancies may be attributed to different dose and duration of FGF21 administration and distinct status of obese animals. In our present study, we demonstrated a bi-phasic change in adipose expression of the FGF21 receptor complexes during the development of dietary obesity: increased at the early stage (4 weeks) and then progressively declined to a hardly detectable level at the late stage (12 weeks). Accordingly, the compromised responses to low-dose FGF21 administration, with respect to the reduction in circulating levels of glucose, insulin, TG, and FFAs, were observed only at the late stage of dietary obesity, whereas the metabolic benefits of high-dose FGF21 remained intact under this circumstance. Collectively, these findings suggest that the sensitivity, but not the maximal responses to FGF21, is impaired in severe dietary obesity, a scenario reminiscent of diabetic patients with insulin resistance who still respond well to therapeutic administration of insulin with rapid decrease of hyperglycemia.

Our present study provides several lines of evidence demonstrating that the protective effects of exercise against obesity-induced insulin resistance and metabolic complications are mediated at least in part by restoration of FGF21 sensitivity in adipose tissues. First, the diminished effects of low-dose FGF21 on reduction of circulating glucose, insulin, TG, and FFAs in the dietary obese mice were largely rectified by exercise, accompanied with restoration of FGF21 signaling and augmented expression of both FGFR1 and KLB in adipose tissues. Second, mice with adipocyte-selective ablation of KLB

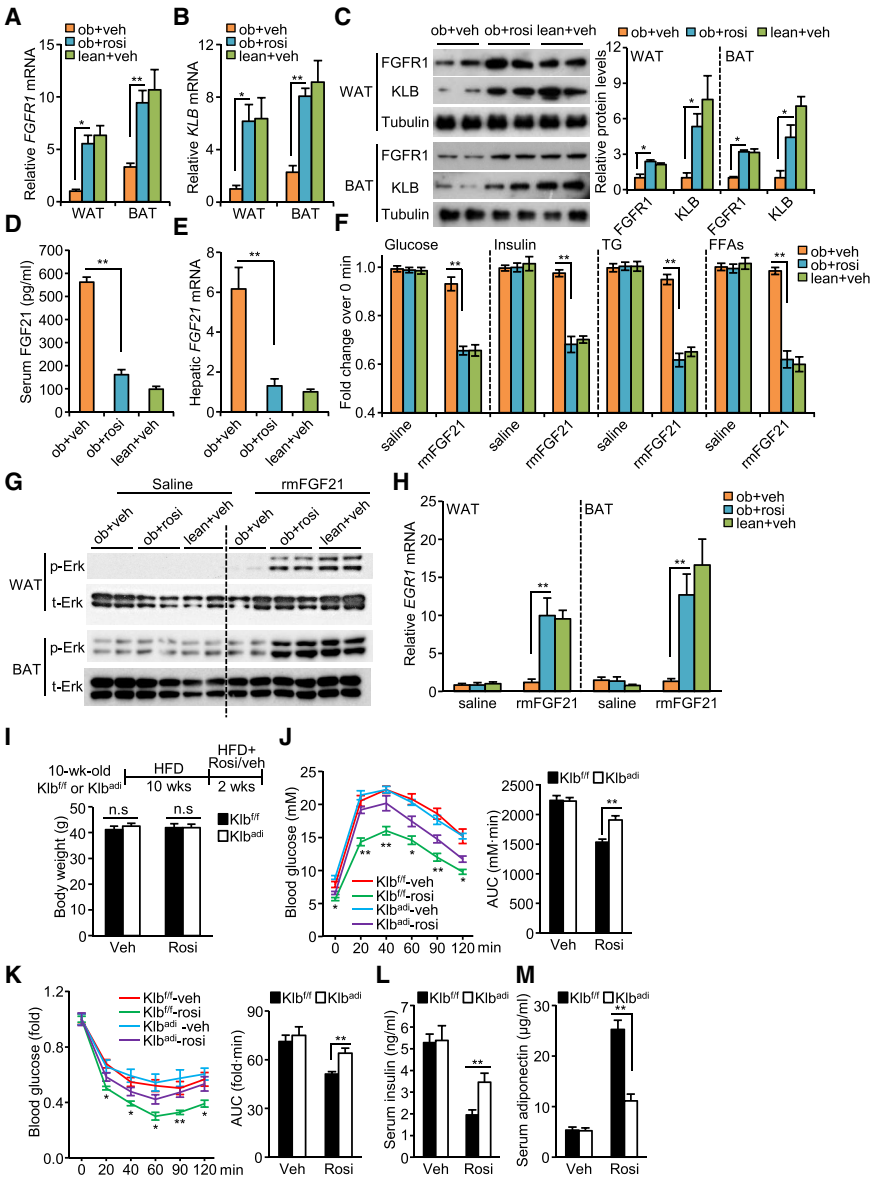

Figure 7. Rosiglitazone Alleviates Diet-Induced Glucose Intolerance And Insulin Resistance By Enhancing FGF21 Sensitivity In Adipose Tissues

For (A)–(H), 10-week-old male C57BL/6J mice were fed with HFD for 12 weeks. During the last 2 weeks, mice were administered with rosiglitazone (ob+rosi, 10 mg/kg body weight) or vehicle (ob+veh, 1% methylcellulose) by daily oral gavage. Mice fed standard chow treated with vehicle were used as lean control (lean+veh). For (I)–(M), 10-week-old male $Klb^{f/f}$ and Klb^{adi} mice were fed with STD (lean) or HFD (obese) for 12 weeks. In the last 2 weeks, mice were treated with 10 mg/kg body weight of rosiglitazone (Rosi) or vehicle (Veh, 1% methylcellulose).

(A and B) Relative *FGFR1* (A) and *KLB* (B) mRNA levels in epididymal WAT and BAT measured by real-time PCR and normalized to *β-actin* gene (n = 5).

(C) Representative immunoblots (top) and densitometric quantification (bottom) of FGFR1 and KLB protein in epididymal WAT and BAT (n = 4). Tubulin, internal control.

(D) Serum FGF21 levels measured by ELISA (n = 8).

(E) Hepatic *FGF21* mRNA levels measured by real-time PCR and normalized to *β-actin* gene (n = 5).

(F) 0.5 mg/kg body weight of rmFGF21 or saline was i.p. injected into mice. Blood glucose and serum levels of insulin, TG, and FFAs were measured at 180 min, 120 min, 120 min, and 90 min after injection respectively. Fold change over basal level (0 min) was calculated (n = 5). The absolute mean ± SEM values of each group are provided in Table S6.

(G and H) Adipose tissues collected at 10 min after mice receiving i.p. injection with 0.5 mg/kg body weight of rmFGF21 or saline were subjected to immunoblotting analysis for total or phosphorylated Erk (Thr202/Tyr204) (G), or collected at 90 min after injection and subjected to real-time PCR analysis for quantification of *EGR1* mRNA levels (H) (n = 5).

(I) Body weight was measured at week 12 (n = 7–9). n.s., not significant.

(J) GTT performed at week 11 and AUC during GTT (n = 7,* $Klb^{f/f}$-rosi versus Klb^{adi}-rosi).

(K) ITT performed at week 12 and AUC during ITT (n = 7, * $Klb^{f/f}$-rosi versus Klb^{adi}-rosi).

(L and M) Serum levels of insulin (L) and adiponectin (M) measured by ELISA at the end of experiment (n = 6–9).

Data are represented as mean ± SEM, *p < 0.05, **p < 0.01. Representative data from three independent experiments are shown.

were resistant to the multiple benefits of exercise on alleviation of obesity-associated systemic insulin resistance, glucose intolerance, dyslipidemia, and fatty liver. Our findings can explain the discrepant changes of circulating FGF21 in response to acute and chronic exercise, as reported in several previous studies. It is likely that the rapid rise of circulating FGF21 after acute exercise in healthy individuals (Kim et al., 2013) represents an adaptive response to handle metabolic stress, whereas the decreased levels of plasma FGF21 after long-term exercise in obese individuals or animals (Fletcher et al., 2012; Yang et al., 2011) as well as in elderly men (Taniguchi et al., 2016) result from attenuation of FGF21 resistance.

Although circulating FGF21 is produced predominantly from the liver (Markan et al., 2014), adipose tissues, but not liver, are the major targets of FGF21 mediating its multiple effects on whole-body metabolic homeostasis and insulin sensitivity (Adams et al., 2012; Ding et al., 2012; Véniant et al., 2012). In rodents, the several therapeutic benefits of FGF21, including alleviation of obesity-related insulin resistance, fatty liver, atherosclerosis, and myocardial infarction are dependent on induction of adiponectin (Holland et al., 2013; Joki et al., 2015; Lin

et al., 2013, 2015). Consistently, pharmacological treatment with FGF21 analogs also leads to a marked elevation of circulating adiponectin in patients with obesity and type-2 diabetes (Gaich et al., 2013; Talukdar et al., 2016). In contrast, these patients exhibit decreased plasma adiponectin (hypoadiponectinemia) despite of increased endogenous circulating levels of FGF21 (Hui et al., 2016). These paradoxical changes can also be explained by FGF21 resistance in adipose tissues under the pathophysiological conditions. Indeed, our present study showed that mice with defective FGF21 signaling in adipocytes are refractory to chronic exercise-induced elevation of circulating adiponectin, accompanied with exacerbation of ectopic lipid accumulation in skeletal muscle and liver. Unlike the FGF21 receptor complexes, adiponectin receptors (adipoR1 and adipoR2) are ubiquitously expressed in almost all the major tissues including liver and skeletal muscle (Yamauchi et al., 2003), where adiponectin induces fatty acid oxidation by activation of AMP-activated protein kinase, thereby leading to combustion of ectopic lipids and insulin sensitization (Yamauchi et al., 2002; Yoon et al., 2006). Indeed, adiponectin has been shown to be an important mediator for exercise training-induced mitochondrial biogenesis in skeletal muscle cells (Iwabu et al., 2010). Taken together, these findings raise the possibility that chronic exercise-induced metabolic benefits in these non-adipose tissues may be partly attributed to elevated circulating adiponectin resulting from FGF21 sensitization in adipocytes. Further studies are needed to define the contribution of elevated adiponectin as a downstream effector of FGF21 sensitization in conferring the metabolic benefits of exercise on non-adipose tissues.

In adipose tissues, FGF21 acts in a feed-forward manner to regulate the activity of the nuclear receptor PPARγ (Dutchak et al., 2012), a master regulator of adipogenesis and adipocyte functions (Lefterova et al., 2014). PPARγ increases both the expression and secretion of adiponectin, which in turn contributes to the therapeutic effects of the PPARγ agonists thiazolidinediones on alleviation of insulin resistance and vascular dysfunction (Chang et al., 2010; Nawrocki et al., 2006). Our present study demonstrated that the effects of exercise on sensitizing adipose actions of FGF21 are mediated by activation of PPARγ, which in turn induces the expression of the FGF21 receptor complexes through direct transactivation of both the *FGFR1* and *KLB* genes in adipocytes. Notably, exercise-induced elevation of PPARγ activity in adipose tissues is markedly diminished in both FGF21$^{-/-}$ and Klb^{adi} mice compared to WT controls, suggesting that exercise triggers the feed-forward activation between the FGF21 signaling cascades and PPARγ in adipocytes, which in turn increase adiponectin secretion and insulin sensitization. However, it remains unclear whether adipose PPARγ is indeed an obligatory mediator for the metabolic benefits of exercise on systemic insulin sensitivity and glucose homeostasis.

In addition to the PPARγ-adiponectin axis, several other adipose actions of FGF21, such as inhibition of lipolysis and inflammation, may also contribute to the metabolic benefits of exercise. Exercise stimulates TG hydrolysis via activating β-adrenergic receptor-mediated lipolytic signaling in adipose tissues, thus providing glycerol and FFAs for non-adipose tissues as energy source (Ogasawara et al., 2015). However, excessive supply of FFAs may lead to ectopic lipid accumulation and lipotoxicity, thus exacerbating insulin resistance (Saponaro et al., 2015). FGF21 has been shown to suppress growth hormone and lipolytic agents-induced lipolysis both *in vitro* and *in vivo* (Arner et al., 2008; Chen et al., 2011b; Li et al., 2009; Park et al., 2016). Consistently, both FGF21$^{-/-}$ and Klb^{adi} mice exhibit a significant exacerbation of exercise-induced lipolysis in adipose tissues and higher amount of ectopic lipid accumulation in liver and skeletal muscle than those exercised WT mice. Therefore, it is likely that FGF21 acts on adipocytes to counterbalance exercise-induced lipolysis, thus preventing excessive flux of FFAs into circulation and other metabolic organs. Additionally, our present study demonstrated that the suppressive effects of chronic exercise on obesity-induced adipose expression of pro-inflammatory cytokines and elevation of their circulating levels are also dependent on FGF21 signaling in adipocytes, suggesting that FGF21 signaling may also mediate the metabolic benefits of exercise through suppression of obesity-induced adipose inflammation. Nevertheless, further studies are needed to clarify whether such anti-inflammatory effects of FGF21 are secondary to activation of the PPARγ-adiponectin axis or via other mechanisms.

In summary, our studies uncovered the reversal of obesity-induced FGF21 resistance in adipose tissue as a mechanism whereby exercise exerts its multiple benefits on systemic insulin sensitivity, metabolic homeostasis, and other non-adipose tissues. Given the difficulties in developing the long-acting and potent recombinant FGF21 analogs for therapeutic applications, our findings raise the possibility that sensitization of adipose actions of FGF21, which is abundantly present in patients with obesity and diabetes, may represent an alternative strategy for treatment of these chronic diseases.

STAR★METHODS

Detailed methods are provided in the online version of this paper and include the following:

- KEY RESOURCES TABLE
- CONTACT FOR REAGENT AND RESOURCE SHARING
- EXPERIMENTAL MODEL AND SUBJECT DETAILS
  - Animals
- METHOD DETAILS
  - Treadmill exercise
  - Animal studies
  - FGF21 response test
  - Biochemical and immunological analysis
  - Construction of the luciferase reporter vectors
  - Fatty acids oxidation assay
  - Glucose and insulin tolerance tests
  - Histological analysis
  - *Ex vivo* assay for lipolysis of adipose tissue
  - Chromatin immunoprecipitation (ChIP)
  - Transfection and luciferase assays
  - Nucleic acid extraction and real time PCR
  - Immunoblotting analysis
- QUANTIFICATION AND STATISTICAL ANALYSIS

SUPPLEMENTAL INFORMATION

Supplemental Information can be found with this article online at https://doi.org/10.1016/j.celrep.2019.02.014.

ACKNOWLEDGMENTS

This work was supported by collaborative research fund (C4024-16W, C7037-17W) and general research fund (17125317) from the Research Grant Council of Hong Kong, Human Frontier Science Program (RGP0024/2017), Qatar National Research Fund (NPRP 6-428-3-113), and Hong Kong HMRF (03144516).

AUTHOR CONTRIBUTIONS

L.G. designed the study, carried out the research, analyzed and interpreted the results, and wrote the manuscript. B.L. designed the study and carried out the research. L.J., Z.H., and J.Z. conducted the experiments. C.R.T., H.D., Y.H., and Z.L. advised the study and data interpretation and reviewed the manuscript. A.X. designed the study and wrote and edited the manuscript.

DECLARATION OF INTERESTS

The authors declare no competing interests.

Received: September 12, 2018
Revised: January 6, 2019
Accepted: February 2, 2019
Published: March 5, 2019

REFERENCES

Adams, A.C., Yang, C., Coskun, T., Cheng, C.C., Gimeno, R.E., Luo, Y., and Kharitonenkov, A. (2012). The breadth of FGF21's metabolic actions are governed by FGFR1 in adipose tissue. Mol. Metab. *2*, 31–37.

Arner, P., Pettersson, A., Mitchell, P.J., Dunbar, J.D., Kharitonenkov, A., and Rydén, M. (2008). FGF21 attenuates lipolysis in human adipocytes - a possible link to improved insulin sensitivity. FEBS Lett. *582*, 1725–1730.

Asrih, M., Altirriba, J., Rohner-Jeanrenaud, F., and Jornayvaz, F.R. (2015). Ketogenic Diet Impairs FGF21 Signaling and Promotes Differential Inflammatory Responses in the Liver and White Adipose Tissue. PLoS ONE *10*, e0126364.

Boström, P.A., Graham, E.L., Georgiadi, A., and Ma, X. (2013). Impact of exercise on muscle and nonmuscle organs. IUBMB Life *65*, 845–850.

Chang, J., Li, Y., Huang, Y., Lam, K.S., Hoo, R.L., Wong, W.T., Cheng, K.K., Wang, Y., Vanhoutte, P.M., and Xu, A. (2010). Adiponectin prevents diabetic premature senescence of endothelial progenitor cells and promotes endothelial repair by suppressing the p38 MAP kinase/p16INK4A signaling pathway. Diabetes *59*, 2949–2959.

Chen, C., Cheung, B.M., Tso, A.W., Wang, Y., Law, L.S., Ong, K.L., Wat, N.M., Xu, A., and Lam, K.S. (2011a). High plasma level of fibroblast growth factor 21 is an Independent predictor of type 2 diabetes: a 5.4-year population-based prospective study in Chinese subjects. Diabetes Care *34*, 2113–2115.

Chen, W., Hoo, R.L., Konishi, M., Itoh, N., Lee, P.C., Ye, H.Y., Lam, K.S., and Xu, A. (2011b). Growth hormone induces hepatic production of fibroblast growth factor 21 through a mechanism dependent on lipolysis in adipocytes. J. Biol. Chem. *286*, 34559–34566.

Chow, W.S., Xu, A., Woo, Y.C., Tso, A.W., Cheung, S.C., Fong, C.H., Tse, H.F., Chau, M.T., Cheung, B.M., and Lam, K.S. (2013). Serum fibroblast growth factor-21 levels are associated with carotid atherosclerosis independent of established cardiovascular risk factors. Arterioscler. Thromb. Vasc. Biol. *33*, 2454–2459.

Coskun, T., Bina, H.A., Schneider, M.A., Dunbar, J.D., Hu, C.C., Chen, Y., Moller, D.E., and Kharitonenkov, A. (2008). Fibroblast growth factor 21 corrects obesity in mice. Endocrinology *149*, 6018–6027.

Couture, J.P., and Blouin, R. (2011). The DLK gene is a transcriptional target of PPARγ. Biochem. J. *438*, 93–101.

D'Antona, G., Ragni, M., Cardile, A., Tedesco, L., Dossena, M., Bruttini, F., Caliaro, F., Corsetti, G., Bottinelli, R., Carruba, M.O., et al. (2010). Branched-chain amino acid supplementation promotes survival and supports cardiac and skeletal muscle mitochondrial biogenesis in middle-aged mice. Cell Metab. *12*, 362–372.

Díaz-Delfín, J., Hondares, E., Iglesias, R., Giralt, M., Caelles, C., and Villarroya, F. (2012). TNF-α represses β-Klotho expression and impairs FGF21 action in adipose cells: involvement of JNK1 in the FGF21 pathway. Endocrinology *153*, 4238–4245.

Ding, X., Boney-Montoya, J., Owen, B.M., Bookout, A.L., Coate, K.C., Mangelsdorf, D.J., and Kliewer, S.A. (2012). βKlotho is required for fibroblast growth factor 21 effects on growth and metabolism. Cell Metab. *16*, 387–393.

Dutchak, P.A., Katafuchi, T., Bookout, A.L., Choi, J.H., Yu, R.T., Mangelsdorf, D.J., and Kliewer, S.A. (2012). Fibroblast growth factor-21 regulates PPARγ activity and the antidiabetic actions of thiazolidinediones. Cell *148*, 556–567.

Fisher, F.M., Chui, P.C., Antonellis, P.J., Bina, H.A., Kharitonenkov, A., Flier, J.S., and Maratos-Flier, E. (2010). Obesity is a fibroblast growth factor 21 (FGF21)-resistant state. Diabetes *59*, 2781–2789.

Fisher, F.M., Kleiner, S., Douris, N., Fox, E.C., Mepani, R.J., Verdeguer, F., Wu, J., Kharitonenkov, A., Flier, J.S., Maratos-Flier, E., and Spiegelman, B.M. (2012). FGF21 regulates PGC-1α and browning of white adipose tissues in adaptive thermogenesis. Genes Dev. *26*, 271–281.

Fletcher, J.A., Meers, G.M., Laughlin, M.H., Ibdah, J.A., Thyfault, J.P., and Rector, R.S. (2012). Modulating fibroblast growth factor 21 in hyperphagic OLETF rats with daily exercise and caloric restriction. Appl. Physiol. Nutr. Metab. *37*, 1054–1062.

Folch, J., Lees, M., and Sloane Stanley, G.H. (1957). A simple method for the isolation and purification of total lipides from animal tissues. J. Biol. Chem. *226*, 497–509.

Fon Tacer, K., Bookout, A.L., Ding, X., Kurosu, H., John, G.B., Wang, L., Goetz, R., Mohammadi, M., Kuro-o, M., Mangelsdorf, D.J., and Kliewer, S.A. (2010). Research resource: Comprehensive expression atlas of the fibroblast growth factor system in adult mouse. Mol. Endocrinol. *24*, 2050–2064.

Gaich, G., Chien, J.Y., Fu, H., Glass, L.C., Deeg, M.A., Holland, W.L., Kharitonenkov, A., Bumol, T., Schilske, H.K., and Moller, D.E. (2013). The effects of LY2405319, an FGF21 analog, in obese human subjects with type 2 diabetes. Cell Metab. *18*, 333–340.

Garekani, E.T., Mohebbi, H., Kraemer, R.R., and Fathi, R. (2011). Exercise training intensity/volume affects plasma and tissue adiponectin concentrations in the male rat. Peptides *32*, 1008–1012.

Ge, X., Chen, C., Hui, X., Wang, Y., Lam, K.S., and Xu, A. (2011). Fibroblast growth factor 21 induces glucose transporter-1 expression through activation of the serum response factor/Ets-like protein-1 in adipocytes. J. Biol. Chem. *286*, 34533–34541.

Görgens, S.W., Eckardt, K., Jensen, J., Drevon, C.A., and Eckel, J. (2015). Exercise and Regulation of Adipokine and Myokine Production. Prog. Mol. Biol. Transl. Sci. *135*, 313–336.

Hale, C., Chen, M.M., Stanislaus, S., Chinookoswong, N., Hager, T., Wang, M., Véniant, M.M., and Xu, J. (2012). Lack of overt FGF21 resistance in two mouse models of obesity and insulin resistance. Endocrinology *153*, 69–80.

He, C., Bassik, M.C., Moresi, V., Sun, K., Wei, Y., Zou, Z., An, Z., Loh, J., Fisher, J., Sun, Q., et al. (2012). Exercise-induced BCL2-regulated autophagy is required for muscle glucose homeostasis. Nature *481*, 511–515.

Holland, W.L., Adams, A.C., Brozinick, J.T., Bui, H.H., Miyauchi, Y., Kusminski, C.M., Bauer, S.M., Wade, M., Singhal, E., Cheng, C.C., et al. (2013). An FGF21-adiponectin-ceramide axis controls energy expenditure and insulin action in mice. Cell Metab. *17*, 790–797.

Hotta, Y., Nakamura, H., Konishi, M., Murata, Y., Takagi, H., Matsumura, S., Inoue, K., Fushiki, T., and Itoh, N. (2009). Fibroblast growth factor 21 regulates lipolysis in white adipose tissue but is not required for ketogenesis and triglyceride clearance in liver. Endocrinology *150*, 4625–4633.

Huang, Z., Zhong, L., Lee, J.T.H., Zhang, J., Wu, D., Geng, L., Wang, Y., Wong, C.M., and Xu, A. (2017). The FGF21-CCL11 axis mediates beiging of white adipose tissues by coupling sympathetic nervous system to type 2 immunity. Cell Metab. *26*, 493–508.

Hui, X., Feng, T., Liu, Q., Gao, Y., and Xu, A. (2016). The FGF21-adiponectin axis in controlling energy and vascular homeostasis. J. Mol. Cell Biol. *8*, 110–119.

Huynh, F.K., Green, M.F., Koves, T.R., and Hirschey, M.D. (2014). Measurement of fatty acid oxidation rates in animal tissues and cell lines. Methods Enzymol. *542*, 391–405.

Inagaki, T., Dutchak, P., Zhao, G., Ding, X., Gautron, L., Parameswara, V., Li, Y., Goetz, R., Mohammadi, M., Esser, V., et al. (2007). Endocrine regulation of the fasting response by PPARalpha-mediated induction of fibroblast growth factor 21. Cell Metab. *5*, 415–425.

Iwabu, M., Yamauchi, T., Okada-Iwabu, M., Sato, K., Nakagawa, T., Funata, M., Yamaguchi, M., Namiki, S., Nakayama, R., Tabata, M., et al. (2010). Adiponectin and AdipoR1 regulate PGC-1alpha and mitochondria by Ca(2+) and AMPK/SIRT1. Nature *464*, 1313–1319.

Joki, Y., Ohashi, K., Yuasa, D., Shibata, R., Ito, M., Matsuo, K., Kambara, T., Uemura, Y., Hayakawa, S., Hiramatsu-Ito, M., et al. (2015). FGF21 attenuates pathological myocardial remodeling following myocardial infarction through the adiponectin-dependent mechanism. Biochem. Biophys. Res. Commun. *459*, 124–130.

Kharitonenkov, A., Wroblewski, V.J., Koester, A., Chen, Y.F., Clutinger, C.K., Tigno, X.T., Hansen, B.C., Shanafelt, A.B., and Etgen, G.J. (2007). The metabolic state of diabetic monkeys is regulated by fibroblast growth factor-21. Endocrinology *148*, 774–781.

Kim, K.H., Kim, S.H., Min, Y.K., Yang, H.M., Lee, J.B., and Lee, M.S. (2013). Acute exercise induces FGF21 expression in mice and in healthy humans. PLoS ONE *8*, e63517.

Kriketos, A.D., Gan, S.K., Poynten, A.M., Furler, S.M., Chisholm, D.J., and Campbell, L.V. (2004). Exercise increases adiponectin levels and insulin sensitivity in humans. Diabetes Care *27*, 629–630.

Kujala, U.M. (2009). Evidence on the effects of exercise therapy in the treatment of chronic disease. Br. J. Sports Med. *43*, 550–555.

Kurosu, H., Choi, M., Ogawa, Y., Dickson, A.S., Goetz, R., Eliseenkova, A.V., Mohammadi, M., Rosenblatt, K.P., Kliewer, S.A., and Kuro-o, M. (2007). Tissue-specific expression of betaKlotho and fibroblast growth factor (FGF) receptor isoforms determines metabolic activity of FGF19 and FGF21. J. Biol. Chem. *282*, 26687–26695.

Lancaster, G.I., and Febbraio, M.A. (2014). The immunomodulating role of exercise in metabolic disease. Trends Immunol. *35*, 262–269.

Lee, S., Choi, J., Mohanty, J., Sousa, L.P., Tome, F., Pardon, E., Steyaert, J., Lemmon, M.A., Lax, I., and Schlessinger, J. (2018). Structures of β-klotho reveal a 'zip code'-like mechanism for endocrine FGF signalling. Nature *553*, 501–505.

Lefterova, M.I., Haakonsson, A.K., Lazar, M.A., and Mandrup, S. (2014). PPARγ and the global map of adipogenesis and beyond. Trends Endocrinol. Metab. *25*, 293–302.

Li, X., Ge, H., Weiszmann, J., Hecht, R., Li, Y.S., Véniant, M.M., Xu, J., Wu, X., Lindberg, R., and Li, Y. (2009). Inhibition of lipolysis may contribute to the acute regulation of plasma FFA and glucose by FGF21 in ob/ob mice. FEBS Lett. *583*, 3230–3234.

Li, H., Dong, K., Fang, Q., Hou, X., Zhou, M., Bao, Y., Xiang, K., Xu, A., and Jia, W. (2013). High serum level of fibroblast growth factor 21 is an independent predictor of non-alcoholic fatty liver disease: a 3-year prospective study in China. J. Hepatol. *58*, 557–563.

Li, H., Wu, G., Fang, Q., Zhang, M., Hui, X., Sheng, B., Wu, L., Bao, Y., Li, P., Xu, A., and Jia, W. (2018). Fibroblast growth factor 21 increases insulin sensitivity through specific expansion of subcutaneous fat. Nat. Commun. *9*, 272.

Liang, Q., Zhong, L., Zhang, J., Wang, Y., Bornstein, S.R., Triggle, C.R., Ding, H., Lam, K.S., and Xu, A. (2014). FGF21 maintains glucose homeostasis by mediating the cross talk between liver and brain during prolonged fasting. Diabetes *63*, 4064–4075.

Lin, Z., Tian, H., Lam, K.S., Lin, S., Hoo, R.C., Konishi, M., Itoh, N., Wang, Y., Bornstein, S.R., Xu, A., and Li, X. (2013). Adiponectin mediates the metabolic effects of FGF21 on glucose homeostasis and insulin sensitivity in mice. Cell Metab. *17*, 779–789.

Lin, Z., Pan, X., Wu, F., Ye, D., Zhang, Y., Wang, Y., Jin, L., Lian, Q., Huang, Y., Ding, H., et al. (2015). Fibroblast growth factor 21 prevents atherosclerosis by suppression of hepatic sterol regulatory element-binding protein-2 and induction of adiponectin in mice. Circulation *131*, 1861–1871.

Loyd, C., Magrisso, I.J., Haas, M., Balusu, S., Krishna, R., Itoh, N., Sandoval, D.A., Perez-Tilve, D., Obici, S., and Habegger, K.M. (2016). Fibroblast growth factor 21 is required for beneficial effects of exercise during chronic high-fat feeding. J. Appl. Physiol. (1985) *121*, 687–698.

Luo, Y., and McKeehan, W.L. (2013). Stressed Liver and Muscle Call on Adipocytes with FGF21. Front. Endocrinol. (Lausanne) *4*, 194.

Markan, K.R., Naber, M.C., Ameka, M.K., Anderegg, M.D., Mangelsdorf, D.J., Kliewer, S.A., Mohammadi, M., and Potthoff, M.J. (2014). Circulating FGF21 is liver derived and enhances glucose uptake during refeeding and overfeeding. Diabetes *63*, 4057–4063.

Ming, A.Y., Yoo, E., Vorontsov, E.N., Altamentova, S.M., Kilkenny, D.M., and Rocheleau, J.V. (2012). Dynamics and Distribution of Klothoβ (KLB) and fibroblast growth factor receptor-1 (FGFR1) in living cells reveal the fibroblast growth factor-21 (FGF21)-induced receptor complex. J. Biol. Chem. *287*, 19997–20006.

Nawrocki, A.R., Rajala, M.W., Tomas, E., Pajvani, U.B., Saha, A.K., Trumbauer, M.E., Pang, Z., Chen, A.S., Ruderman, N.B., Chen, H., et al. (2006). Mice lacking adiponectin show decreased hepatic insulin sensitivity and reduced responsiveness to peroxisome proliferator-activated receptor gamma agonists. J. Biol. Chem. *281*, 2654–2660.

Ogasawara, J., Izawa, T., Sakurai, T., Sakurai, T., Shirato, K., Ishibashi, Y., Ishida, H., Ohno, H., and Kizaki, T. (2015). The Molecular Mechanism Underlying Continuous Exercise Training-Induced Adaptive Changes of Lipolysis in White Adipose Cells. J. Obes. *2015*, 473430.

Park, J.G., Xu, X., Cho, S., Hur, K.Y., Lee, M.S., Kersten, S., and Lee, A.H. (2016). CREBH-FGF21 axis improves hepatic steatosis by suppressing adipose tissue lipolysis. Sci. Rep. *6*, 27938.

Pascual, G., Fong, A.L., Ogawa, S., Gamliel, A., Li, A.C., Perissi, V., Rose, D.W., Willson, T.M., Rosenfeld, M.G., and Glass, C.K. (2005). A SUMOylation-dependent pathway mediates transrepression of inflammatory response genes by PPAR-gamma. Nature *437*, 759–763.

Patel, V., Adya, R., Chen, J., Ramanjaneya, M., Bari, M.F., Bhudia, S.K., Hillhouse, E.W., Tan, B.K., and Randeva, H.S. (2014). Novel insights into the cardio-protective effects of FGF21 in lean and obese rat hearts. PLoS ONE *9*, e87102.

Petridou, A., Tsalouhidou, S., Tsalis, G., Schulz, T., Michna, H., and Mougios, V. (2007). Long-term exercise increases the DNA binding activity of peroxisome proliferator-activated receptor gamma in rat adipose tissue. Metabolism *56*, 1029–1036.

Polak, J., Bajzova, M., and Stich, V. (2008). Effect of exercise on lipolysis in adipose tissue. Future Lipidol. *3*, 557–572.

Reilly, S.M., and Saltiel, A.R. (2017). Adapting to obesity with adipose tissue inflammation. Nat. Rev. Endocrinol. *13*, 633–643.

Ruschke, K., Fishbein, L., Dietrich, A., Klöting, N., Tönjes, A., Oberbach, A., Fasshauer, M., Jenkner, J., Schön, M.R., Stumvoll, M., et al. (2010). Gene expression of PPARgamma and PGC-1alpha in human omental and subcutaneous adipose tissues is related to insulin resistance markers and mediates beneficial effects of physical training. Eur. J. Endocrinol. *162*, 515–523.

Samms, R.J., Cheng, C.C., Kharitonenkov, A., Gimeno, R.E., and Adams, A.C. (2016). Overexpression of β-Klotho in Adipose Tissue Sensitizes Male Mice to Endogenous FGF21 and Provides Protection From Diet-Induced Obesity. Endocrinology *157*, 1467–1480.

Saponaro, C., Gaggini, M., Carli, F., and Gastaldelli, A. (2015). The Subtle Balance between Lipolysis and Lipogenesis: A Critical Point in Metabolic Homeostasis. Nutrients *7*, 9453–9474.

Stanford, K.I., Middelbeek, R.J., and Goodyear, L.J. (2015a). Exercise Effects on White Adipose Tissue: Beiging and Metabolic Adaptations. Diabetes *64*, 2361–2368.

Stanford, K.I., Middelbeek, R.J., Townsend, K.L., Lee, M.Y., Takahashi, H., So, K., Hitchcox, K.M., Markan, K.R., Hellbach, K., Hirshman, M.F., et al. (2015b). A novel role for subcutaneous adipose tissue in exercise-induced improvements in glucose homeostasis. Diabetes *64*, 2002–2014.

Talukdar, S., Zhou, Y., Li, D., Rossulek, M., Dong, J., Somayaji, V., Weng, Y., Clark, R., Lanba, A., Owen, B.M., et al. (2016). A Long-Acting FGF21 Molecule, PF-05231023, Decreases Body Weight and Improves Lipid Profile in Non-human Primates and Type 2 Diabetic Subjects. Cell Metab. *23*, 427–440.

Taniguchi, H., Tanisawa, K., Sun, X., Kubo, T., and Higuchi, M. (2016). Endurance Exercise Reduces Hepatic Fat Content and Serum Fibroblast Growth Factor 21 Levels in Elderly Men. J. Clin. Endocrinol. Metab. *101*, 191–198.

Thompson, D., Karpe, F., Lafontan, M., and Frayn, K. (2012). Physical activity and exercise in the regulation of human adipose tissue physiology. Physiol. Rev. *92*, 157–191.

Véniant, M.M., Hale, C., Helmering, J., Chen, M.M., Stanislaus, S., Busby, J., Vonderfecht, S., Xu, J., and Lloyd, D.J. (2012). FGF21 promotes metabolic homeostasis via white adipose and leptin in mice. PLoS ONE *7*, e40164.

Yamauchi, T., Kamon, J., Minokoshi, Y., Ito, Y., Waki, H., Uchida, S., Yamashita, S., Noda, M., Kita, S., Ueki, K., et al. (2002). Adiponectin stimulates glucose utilization and fatty-acid oxidation by activating AMP-activated protein kinase. Nat. Med. *8*, 1288–1295.

Yamauchi, T., Kamon, J., Ito, Y., Tsuchida, A., Yokomizo, T., Kita, S., Sugiyama, T., Miyagishi, M., Hara, K., Tsunoda, M., et al. (2003). Cloning of adiponectin receptors that mediate antidiabetic metabolic effects. Nature *423*, 762–769.

Yang, S.J., Hong, H.C., Choi, H.Y., Yoo, H.J., Cho, G.J., Hwang, T.G., Baik, S.H., Choi, D.S., Kim, S.M., and Choi, K.M. (2011). Effects of a three-month combined exercise programme on fibroblast growth factor 21 and fetuin-A levels and arterial stiffness in obese women. Clin. Endocrinol. (Oxf.) *75*, 464–469.

Yoon, M.J., Lee, G.Y., Chung, J.J., Ahn, Y.H., Hong, S.H., and Kim, J.B. (2006). Adiponectin increases fatty acid oxidation in skeletal muscle cells by sequential activation of AMP-activated protein kinase, p38 mitogen-activated protein kinase, and peroxisome proliferator-activated receptor alpha. Diabetes *55*, 2562–2570.

Zhang, X., Yeung, D.C., Karpisek, M., Stejskal, D., Zhou, Z.G., Liu, F., Wong, R.L., Chow, W.S., Tso, A.W., Lam, K.S., and Xu, A. (2008). Serum FGF21 levels are increased in obesity and are independently associated with the metabolic syndrome in humans. Diabetes *57*, 1246–1253.

STAR★METHODS

KEY RESOURCES TABLE

REAGENT or RESOURCE	SOURCE	IDENTIFIER
Antibodies		
Rabbit monoclonal anti-FGF Receptor 1 (D8E4)	CST	Cat#9740; RRID: AB_11178519
Rabbit anti-p44/42 MAP kinase (phosphorylated Erk1/2)	CST	Cat#9101; RRID: AB_331646
Rabbit polyclonal anti-p44/42 MAPK (Erk1/2)	CST	Cat#9102; RRID: AB_330744
Rabbit polyclonal anti-Phospho-Akt (Ser473)	CST	Cat#9271; RRID: AB_329825
Rabbit polyclonal anti-Akt	CST	Cat#9272; RRID: AB_329827
Rabbit polyclonal anti-Phospho-HSL (Ser660)	CST	Cat#4126; RRID: AB_490997
Rabbit polyclonal anti-HSL	CST	Cat#4107; RRID: AB_2296900
Rabbit monoclonal anti-ATGL (30A4)	CST	Cat#2439; RRID: AB_2167953
Goat polyclonal anti-betaKlotho, Unconjugated, Clone E-17	Santa Cruz	Cat#sc-74343, RRID: AB_2265371
Rabbit monoclonal anti-PPARgamma (H-100)	Santa Cruz	Cat#sc-7196x; RRID: AB_654710
Rabbit polyclonal anti-beta Tubulin	Abcam	Cat#ab15568; RRID: AB_2210952
Rabbit polyclonal anti-Adiponectin	Immunodiagnostics Limited	Cat#12010
Bacterial and Virus Strains		
DH5α competent *E. coli*	ThermoFisher	Cat#18265017
Chemicals, Peptides, and Recombinant Proteins		
Recombinant mouse FGF21 protein	Immunodiagnostics Limited	Cat#42189
Rosiglitazone	Biochempartner	Cat#122320734
GW9662	Sigma	Cat#M6191
^{14}C-labeled palmitic acid	PerkinElmer	Cat#NEC075H
D-Glucose	Sigma	Cat#G5767
Insulin	Novo Nordisk	Actrapid® HM
Oil Red O	Sigma	Cat#O0625
Protease inhibitor cocktail tablets	Roche	Cat#04693159001
Proteinase K	NEB	Cat#P8107S
RNAiso Plus	Takara	Cat#9109
PrimeScript RT reagent kit	Takara	Cat#RR037A
SYBR Premix Ex Taq	Takara	Cat#RR420D
Critical Commercial Assays		
TG Determination Kit	Stanbio Laboratory	Cat#2200-225
FFAs, Half Micro Test	Roche	Cat#11383175001
Mouse FGF21 ELISA Kit	Immunodiagnostics Limited	Cat#32180
Mouse Insulin ELISA Kit	Immunodiagnostics Limited	Cat#32270
Mouse Adiponectin ELISA Kit	Immunodiagnostics Limited	Cat#32010
Mouse TNF-α ELISA Kit	R&D	Cat#MTA00B
Mouse IL-1β ELISA Kit	R&D	Cat#MLB00C
BCA Assay Kit	Pierce	Cat#23225
Free Glycerol Reagent	Sigma	Cat#F6428
Experimental Models: Organisms/Strains		
C57BL/6J mouse	The Jackson Laboratory	Stock No: 000664
FGF21 KO mouse	Hotta et al., 2009	N/A
KLB-floxed mouse	Shanghai Model Organisms Center,Inc.	N/A
B6;FVB-Tg (Adipoq-cre) 1Evdr/J (adiponectin-Cre)	The Jackson Laboratory	Stock No: 010803

(*Continued on next page*)

Continued

REAGENT or RESOURCE	SOURCE	IDENTIFIER
Oligonucleotides		
Primer used in this study (see Table S7)	This paper	N/A
Recombinant DNA		
pGL3-Basic Vector	Addgene	Cat#E1751
Murine *FGFR1* promoter -Luciferase plasmid	This paper	N/A
Murine *KLB* promoter-Luciferase plasmid	This paper	N/A
Software and Algorithms		
GraphPad Prism 7	GraphPad software	https://www.graphpad.com/
Excel	Microsoft Office 365	https://www.office.com/
ImageJ	National Institutes of Health (NIH)	https://imagej.nih.gov/ij/
Other		
Standard chow diet	LabDiet	Cat#5053
High fat diet	Research Diets	Cat#D12451

CONTACT FOR REAGENT AND RESOURCE SHARING

Further information and requests for resources and reagents should be directed to and will be fulfilled by the Lead Contact, Aimin Xu (amxu@hku.hk).

EXPERIMENTAL MODEL AND SUBJECT DETAILS

Animals

FGF21-KO (FGF21$^{-/-}$) mice and KLB-floxed (Klb$^{f/f}$) mice were generated as previously described (Hotta et al., 2009; Lin et al., 2015). Adiponectin-cre (Jackson Laboratory) mice were used to generate adipose tissue-specific KLB-KO (Klb^{adi}) mice (Li et al., 2018). 10-week-old male mice were housed in Laboratory Animal Unit at controlled temperature (23 ± 1°C) with a 12-hour light-dark cycle and free access to water and diet (either standard chow or a high fat diet, Research Diets #D12451). Body composition was monitored using the Bruker Minispec LF90 II Body Composition Analyzer (Bruker Biospin, USA). All experiments were conducted with male mice and were approved by the Committee on the Use of Live Animals in Teaching & Research at the University of Hong Kong (HKU).

METHOD DETAILS

Treadmill exercise

Mice were acclimated to treadmill (LE8710M, Panlab, Spain) running at a low speed for 2 days as previously described (He et al., 2012) and then trained on the treadmill with 10° uphill incline at a changing speed for one section (Acclimation stage: 10 cm/s for 5 minutes; Acceleration stage: speed was increased at a rate of 1 cm/s/min to 20 cm/s; Maintaining stage: 20 cm/s for 20 min; Deceleration stage: speed was reduced at a rate of 4 cm/s/min). The mice were daily trained for 5 days per week.

Animal studies

For treadmill exercise training, 10-week-old male mice were fed with HFD for 8 weeks, and were then randomly divided into exercise and non-exercise groups. To evaluate the roles of PPARγ on the effects of exercise in FGF21 sensitivity, mice on HFD for 8 weeks as above were administrated with 10 mg/kg body weight of GW9662 (Sigma#M6191), 10 mg/kg body weight of rosiglitazone (Biochempartner#122320734, Shanghai, China) or vehicle (1% methylcellulose) by daily oral gavage for 2 or 4 weeks.

FGF21 response test

Mice were i.p injected with 0.5mg/kg or 5mg/kg body weight endotoxin-free tagless rmFGF21 protein (Immunodiagnostics Limited#42189, HK) or saline control after 3h of fasting (8:00am-11:00am). Blood was collected from tail vein at various time points for further analysis. Adipose tissues were collected at 15min or 90min after injection to check Erk phosphorylation or *EGR1* mRNA expression levels respectively.

Biochemical and immunological analysis

Blood glucose was measured using an Accu-Check blood glucose meter (Roche, Germany). Serum TG and ALT concentrations were quantified using commercial kits (Stanbio Laboratory, USA). Serum FFAs concentrations were measured with the FFAs, Half Micro

Test (Roche, Germany). For tissue TG and FFAs measurements, total lipid was extracted from approximately 50mg liver or gastrocnemius muscle as previously described (Folch et al., 1957). Serum levels of FGF21, insulin, and adiponectin were measured with ELISA kits prepared in house (Immunodiagnostics Limited#32180, 32270 and 32010, HK). Serum levels of TNF-α and IL-1β were measured with ELISA kits from R&D (#MTA00B, #MLB00C).

Construction of the luciferase reporter vectors

The murine *FGFR1* promoter region spanning −1972/+3 and *KLB* promoter region spanning −1954 /+21 were amplified from C57BL/6J mouse genomic DNA and then sub-cloned into pGL3-Basic (pGL3B) vector using NheI and HindIII sites. Nucleotide sequences of the 5′-flanking regions of *FGFR1* and *KLB* promoter were scanned, and two putative PPARγ binding sites (PPREs) were identified in each promoter region. The core sequences of PPREs (5′-AAAG-3′) within the promoter region were mutated to 5′-GCCA-3′ by a DpnI-based site-directed mutagenesis method. All the constructs were confirmed by automatic DNA sequencing. The primers used for the vector construction are listed in Table S7. The PPARγ expression plasmid was a gift from Christopher K. Glass (Pascual et al., 2005).

Fatty acids oxidation assay

Liver and muscle fatty acids oxidation (FAO) capacities were measured using ^{14}C-labeled palmitic acid (PerkinElmer#NEC075H) oxidation assay as previously described (Huynh et al., 2014). Fresh tissues (approximately 200mg liver and 160mg gastrocnemius muscle) were washed with chilled PBS and homogenized in a Dounce homogenizer containing 1ml chilled STE buffer (0.25M sucrose, 10mM Tris-HCl and 1mM EDTA, pH 7.4). The crude homogenates were briefly centrifuged and the supernatant containing crude mitochondria was collected for further reaction. The reactions were started by mixing 30 μL tissue homogenate with 370 μL oxidation reaction buffer (100mM sucrose, 10mM Tris-HCl, 5mM KH_2PO_4, 0.2mM EDTA, 80mM KCl, 1mM $MgCl_2$, 2mM L-carnitine, 0.1mM malate, 0.05mM Co-enzyme A, 2mM ATP, 1mM dithiothreitol, 0.5mM palmitate, 0.7% BSA, and 0.4 μCi ^{14}C-palmitate), followed by incubation at 37°C for 30min. The reactions were stopped with 200 μL 1M perchloric acid and the $^{14}CO_2$ was captured using Whatman paper disc containing 20 μL 1M NaOH for 1h at room temperature. The radioactivity was counted in 4ml scintillation fluid (American Biosciences#NACS104) with Packard Cobra II Auto Gamma Counter and normalized to the weight of tissues.

Glucose and insulin tolerance tests

Glucose tolerance test was performed in overnight-fasted (19:00pm-9:00am) mice by an intraperitoneal injection of D-glucose (Sigma#G5767, 2g/kg body weight). Insulin tolerance test was conducted with an intraperitoneal injection of insulin (Actrapid® HM, 1U/kg body weight) to mice after 6h of fasting (8:00am-14:00pm). The blood was collected from tail vein at various time points as specified in each experiment for measurement of glucose levels with an Accu-Check blood glucose meter.

Histological analysis

For hematoxylin and eosin (H&E) staining, liver and adipose tissue specimens were fixed in 10% formalin solution at 4°C overnight, processed by LEICA ASP200S tissue processor and embedded in paraffin. After being embedded in paraffin wax, 5 μm sections of liver and adipose tissues were cut and mounted onto gelatin-coated slides. The sections were incubated in HistoChoice for 15min each for 3 times, followed by dehydration in 100%, 90%, 80% and 70% ethanol for 3min respectively. The nuclei were stained with the hematoxylin for 60 s. Afterward, the sections were rinsed in tap water for 10min, and stained with eosin for 30 s, followed by dehydration in 100% ethanol for 5 min and incubation for 30min in xylene. The sections were then mounted in histofluid mounting medium (Paul Marienfeld#6900002). For Oil Red O staining, the fresh liver tissues were embedded in OCT (Tissue-Tek, Sakura Finetek, USA) and cut at 8 μm in the cryostat at −13°C. The sections were briefly fixed in formalin, washed with running tap water for 8min, were then rinsed with 60% isopropanol and stained with freshly-prepared Oil Red O working solution (0.3% Oil Red O (Sigma#O0625) in isopropanol) for 15min. Afterward, the sections were rinsed with 60% isopropanol and lightly stained the nuclei with hematoxylin 5 dips. All slides were examined under Nikon NI-SS biological microscope (Nikon, Japan) and images were captured using a RT3 Slider digital camera system (Diagnostic, USA).

Ex vivo assay for lipolysis of adipose tissue

Approximately 100mg fresh epididymal adipose tissue dissected from mice was washed with cold PBS and minced into small pieces (about 3mm × 3mm). The excised adipose tissue explants were cultured in 500 μL phenol red frees DMEM (Invitrogen#11054) containing 0.5% fatty acids free BSA and 5.56mM D-glucose at 37°C for 24h. Afterward, 10 μL conditioned medium was harvested for measurement of glycerol using Free Glycerol Reagent (Sigma#F6428) as previously described (Chen et al., 2011b). At last, the adipose tissue explants were homogenized in 600 μL cold STE buffer (0.25M sucrose, 10mM Tris-HCl and 1mM EDTA, pH 7.4) using an electric tissue homogenizer for 8min. Cell debris was removed by centrifugation at 12, 000rpm for 10min. Protein concentration in cell extracts was determined by BCA assay kit (Pierce#23225). The glycerol release in each sample was normalized to the protein concentration.

Chromatin immunoprecipitation (ChIP)

3T3-L1 mouse fibroblasts grown in 10-cm plates were differentiated into adipocytes using a differentiation protocol (Lin et al., 2013). ChIP assays were conducted at different days after induction for differentiation as described (Couture and Blouin, 2011). Briefly, cells

were cross-linked with 8ml 1% formaldehyde in PBS for 10min at room temperature, washed in cold PBS, and then resuspended in 250 μL of ChIP lysis buffer (1% SDS, 10mM EDTA, 50mM Tris-HCl, pH 8.0, and protease inhibitor cocktails) by sonication (30% maximum output for 15 s with 3min pause, four cycles) in an ice bath. A 5% portion of the lysates was used for purification of total DNA. The remaining lysates were incubated with 10 μg rabbit polyclonal PPARγ antibody (sc-7196x, Santa Cruz) or non-immune rabbit IgG (control) at 4°C overnight. The immunocomplexes were precipitated using protein A agarose (Pierce#20333) coated with herring sperm DNA (Invitrogen#15634017) and washed sequentially with the following buffers: low-salt wash buffer (0.1% SDS, 1% Triton X-100, 2mM EDTA, 20mM Tris-HCl, pH 8.1, and 150mM NaCl); high-salt wash buffer (0.1% SDS, 1% Triton X-100, 2mM EDTA, 20mM Tris-HCl, pH 8.1, and 500mM NaCl); LiCl wash buffer (0.25M LiCl, 1% NP40, 1% sodium deoxycholate, 1mM EDTA and 10mM Tris-HCl, pH 8.1); and TE solution (10mM Tris-HCl, pH 8.0, and 1mM EDTA). DNA–protein complexes were reversed by incubation at 65°C overnight, followed by Proteinase K (NEB#P8107S) treatment. DNA was recovered by purification using phenol-chloroform methods and was subjected to real time PCR analysis with primers spanning the predicted PPRE regions in the promoter of the *FGFR1* or *KLB* gene. A site located about 6kb upstream of the *FGFR1* or *KLB* transcription starting site was amplified as a negative control region. The large ribosomal protein p0 (36B4) nuclear gene was also quantified as an internal control for total input DNA. The primer sequences used are listed on the Table S7.

Transfection and luciferase assays

For transient transfection assays, HEK293 cells were maintained in DMEM containing 10% fetal bovine serum supplemented with antibiotics. Cells were plated in 24-well plates and transfected with a firefly reporter vector (0.2 μg) and Renilla reporter vector (0.01 μg), together with indicated expression plasmids (0.2 μg) using Polyethylenimine (Polysciences#23966) transfection reagent when cells had grown up to 90% confluence. After transfection for 48h, cells were solubilized in a lysis buffer (Promega#E1500), and luciferase activity was measured with CLARIOstar 0430 Microplate Reader from BMG LABTECH. Firefly luciferase activity was normalized to Renilla luciferase activity.

Nucleic acid extraction and real time PCR

Total RNA was extracted from cells or tissues using RNAiso Plus reagent (Takara#9109). cDNA was synthesized from RNA (500ng) by reverse transcription with PrimeScript RT reagent kit (Takara#RR037A) with random primers. Real time PCR reactions (25ng cDNA, 250nM each primer and 5ul SYBR Premix Ex Taq (Takara#RR420D). All reactions were performed in triplicate on the Applied Biosystems Prism 7000 sequence detection system. The level of target gene expression was normalized against the *β-actin* gene. For mitochondrial DNA quantification, total DNA was extracted from tissue using phenol-chloroform methods. Mitochondrial DNA was amplified using primers specific for the mitochondrial cytochrome B (*CytB*) gene and normalized to genomic DNA by amplification of the large ribosomal protein p0 (*36B4*) nuclear gene as previously described (D'Antona et al., 2010). The specific primers used in this study are listed in Table S7.

Immunoblotting analysis

Proteins were extracted from cells or tissues using RIPA buffer (150mM sodium chloride, 1.0% NP-40, 0.5% sodium deoxycholate, 0.1% SDS, 50mM Tris-HCl, pH 8.0) containing protease inhibitors cocktail (Roche#04693159001), resolved by SDS-PAGE, and then transferred to PVDF membranes (Millipore#IPVH00010). The membranes were then probed with primary antibodies followed by incubation with corresponding HRP-conjugated secondary antibodies. The protein bands were visualized with enhanced chemiluminescence reagents under the ChemiDoc™ MP Imaging System and quantified with the ImageJ software.

QUANTIFICATION AND STATISTICAL ANALYSIS

Statistical analysis was performed using Prism (GraphPad) and Microsoft Excel. Values were expressed as mean ± SEM. Statistical significance was determined by Student's t test (for comparison of two experimental conditions) or ANOVA (for comparison of three or more experimental conditions). In all statistical comparisons, p values less than 0.05 were considered to indicate statistically significant differences. Significance and n values can be found in the figure legends.